CHAPTER 1: INTRODUCTION

1.0 General

Soft marine clays are found along the east coast of Queensland. This material is typically found in coastal plain landforms; for example mudflats and swamps. Many of the roads located along the eastern coast transverse such landforms.

In 1995 the Queensland Department of Main Roads (QDMR) built a trial road embankment along the Gold Coast Highway. The embankment is located near the Coombabah Creek Bridge in a marine environment. Constructed on a soft organic clay layer the embankment was installed with instrumentation to monitor its performance.

The trial embankment was divided into three sections, section one had no ground improvement while the other two sections utilised ground improvement techniques (stone columns). The purpose was to assess the efficiency of stone columns in both reducing and accelerating the settlement of the soft organic clay.

1.1 Scope and Objectives

1.1.1 Scope of Research

During the early stages of this thesis, it was proposed that the trial embankments built along the Port of Brisbane Motorway and Gold Coast Highway be analysed. Due to time limitations, only one of these locations could be analysed. The trial embankment built along the Gold Coast Highway was selected. Focusing on only one embankment has allowed the Author to conduct a more thorough investigation.

This undergraduate thesis analyses the performance of the Coombabah Creek trial embankment. The data used in this thesis was obtained from the QDMR Geotechnical Services Branch at Herston. This data was not structured. Essential information was missing from all reports, for example the actual construction schedule. Considerable time was spent by the Author organising the data into a systematic structure.

The Queensland Department of Main Roads is a state government organisation not a private company. As records were not comprehensive and complete, it was difficult for the Geotechnical staff to be of much assistance to the project or the Author. For these reasons numerous assumptions had to be made when analysing the performance of the trial embankment.

All the raw data obtained from the QDMR was replotted by the Author. The longitudinal soil profile and embankment geometry was redrawn using AutoCAD 2004. The Author created his own intellectual property to solve the finite difference consolidation equations. Knowledge gained from engineering mathematics courses was utilised to solve these difficult expressions.

The following two commercial Geotechnical Engineering computer programs were used in this thesis – Slope/W and Plaxis. All Slope/W models contained within the thesis were produced by the Author. Considerable time and effort was spent reading the Slope/W user manual to gain a basic understanding of the software. The Author encountered many difficulties when modelling the trial embankment on Plaxis. With only the user manual and overseas Plaxis experts to consult, it was very difficult to model the embankment correctly in such a short thesis time frame. Thus external assistance was drawn upon to model the embankment on Plaxis.

1.1.2 Objectives

The aim of this thesis is to analyse the extensive laboratory and field data that exists on the trial embankment built near the Coombabah Creek Bridge. This can be achieved by completing the following steps:

. • Analyse data obtained from the Queensland Department of Main Roads

. • Compare the monitored field performance against the expected behaviour, as envisaged during the design stage, with our current understanding of soft clay behaviour

. • Compare the back-calculated geotechnical parameters obtained from large scaled field tests and those obtained from small scale single element laboratory tests

. • Compare the observed and predicted data with that from existing numerical analysis tools such as Plaxis

1.2 Outline of Thesis

This undergraduate thesis is divided into five chapters. Chapter 1 contains background information of the research area, the thesis objectives and scope and outline. Chapter 2 is an extensive literature review on ground improvement techniques used in road embankments. Chapter 3 contains the soil characteristics at the site where the trial embankment was constructed. Included in this chapter are the in-situ conditions before the embankment is constructed and the subsequent conditions after the embankment is constructed. Chapter 4 includes a detailed analysis of all laboratory and instrumentation data and computer analysis outputs. Chapter 5 provides a conclusion of the effectiveness of the ground improvement technique (stone columns). Recommendation for future developments will also be provided.

CHAPTER 2: LITERATURE REVIEW

2.0 Introduction

In chapter 2 an extensive literature review is conducted on ground improvement techniques used in road embankments. During the initial stages of the thesis, when the Port of Brisbane Motorway was to be analysed, literature was reviewed on prefabricated vertical drains. In the later stages of this thesis, when it was decided just to analyse the Coombabah Creek trial embankment, the performance of stone columns was investigated. The work of researchers, in these fields, is considered and mathematical models explaining the behaviour of the ground improvement techniques are discussed.

2.1 General

Soft marine clays are spread along the east coast of Queensland. This material is generally found in coastal plain areas such as mudflats and swamp lands. Many of the major roads located along the eastern coast belt of Queensland pass through these landforms. Construction of new roads or the widening of existing roads, on sensitive marine clays, poses many difficulties. The stability of this brittle material is very difficult to control during construction. Earthwork contractors are given little or no warning prior to failure (Wijeyakulasuriya et al., 1999). Soft marine clays are also known for their low strength and highly compressible nature. To enhance the constructability of these sites, ground improvement techniques are typically employed.

For more than two decades the Geotechnical Group at the Queensland Department of Main Roads (QDMR) have been exploring the benefits of soil improvement techniques. They have built trial road embankments which stretch from the Gold Coast to as far north as Mackay in North Queensland. This literature review will offer greatest insight into the trial embankments built by the QDMR. Other soil improvement techniques will also be briefly discussed.

2.2 Ground Improvement

Pre-loading in combination with prefabricated vertical drains (PVD) and stone columns was used by the Main Roads in constructing trial embankments along the Port of Brisbane Motorway (near the Gateway Bridge) and the Gold Coast Highway (near the Coombabah Creek Bridge) respectively. These ground improvement techniques were used to improve the structural properties of the foundation material.

Deep mixing method is an alternative method of improving the structural properties of roads built on soft marine clays.

2.3 Preloading

Preloading is one of the oldest methods of stabilising soft clays. It involves loading the ground with fill material, to compress underlying stratum. The main objective in pre-compression is to reduce the magnitude of settlement after construction. Mitchell presented an expression to determine the settlement at any time after construction (Mitchell, 1981) –

$$s_t = s_i + \overline{U}s_{cons} + s_s \quad (2.1)$$

The required settlement can be determined by either establishing the magnitude of the preload pressure required to produce the desired settlement within the specified time, or, establishing the time required to achieve a given amount of settlement under a given preload.

In 1977, Olson presented a mathematical solution to determine the degree of consolidation under a time dependant load (Braja, 1983) –

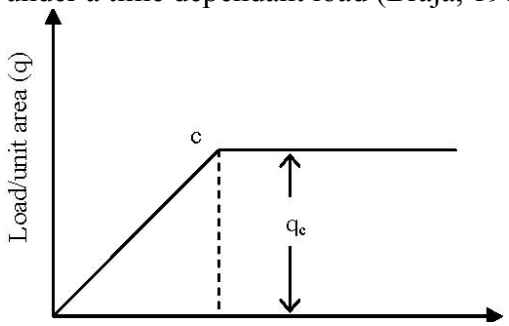

Figure 2.1: One dimensional consolidation due to a single ramp load

For $T_v \leq T_c$:

$$u_e = \sum_{m=0}^{m=\infty} \frac{2q_c}{M^3 T_c} \sin\frac{Mz}{H}\left[1-\exp\left(-M^2T_v\right)\right] \quad (2.2)$$

$$U_{av} = \frac{T_v}{T_c}\left[1-\frac{2}{T_v}\sum_{m=0}^{m=\infty}\frac{1}{M^4}\left[1-\exp\left(-M^2T_v\right)\right]\right] \quad (2.3)$$

For $T_v > T_c$:

$$u_e = \sum_{m=0}^{m=\infty} \frac{2q_c}{M^3 T_c}\left[\exp\left(M^2T_c\right)-1\right]\sin\frac{Mz}{H}\exp\left(-M^2T_v\right) \quad (2.4)$$

$$U_{av} = 1-\frac{2}{T_c}\sum_{m=0}^{m=\infty}\frac{1}{M^4}\left[\exp\left(M^2T_c\right)-1\right]\exp(-M^2T_v) \quad (2.5)$$

Olson's solution assumes that the weight of an embankment applies a uniformly distributed load (qc) to the ground surface. This load varies linearly with time, until the embankment is fully constructed (Figure 2.1 Point "c").
Two expressions have been formulated by Olson to determine the average degree of consolidation (Uav). When Tv ≤ Tc the degree of consolidation (Uav) varies with the time factor (Tv) during the phase when the load increases linearly with construction. When the Tv > Tc the embankment is fully constructed and the degree of consolidation is given by equation (2.5).

2.4 Prefabricated Vertical Drains (PVD)

The time required to compress soft marine clays by preloading alone is excessive. Prefabricated vertical drains are commonly installed to accelerate the rate of pore water dissipation. This inturn increases the rate of settlement and hence reduces the time required to compress the clay stratum.
PVDs are very effective in accelerating the rate of consolidation, if the horizontal coefficient of consolidation (Ch) is much greater than the vertical (Cv). This is because vertical drains considerably reduce the drainage path in the radial direction.
Vertical drains are suitable for moderately to highly compressible soils, which are usually normally consolidated or lightly consolidated, and for stabilising a deep layer of soft clay having a low permeability (Indraratna et al., 2003).

2.4.1 PVD Structure

Prefabricated band-shaped drains and Kjellman cardboard wick drains were introduced as ground improvement techniques in 1940. Since then, several other types of PVD have been developed which include the Geodrain (Sweden), Alidrain (England) and Mebradrain (Netherlands).
Prefabricated vertical drains are composed of a perforated plastic core functioning as a drain, and a protective sleeve of fibrous material as a filter around the core. The typical dimension of band drains is 3.5 mm x 100 mm (Indraratna et al., 2003).

2.4.2 Installation of PVD

Generally vertical drains are installed using either the dynamic or static method. The dynamic method involves driving a steel mandrel into the ground using either a vibrating hammer or conventional drop hammer. The static method involves pushing the mandrel into the ground, by means of a static force.
The disadvantage of the dynamic method is that it causes disturbance of the surrounding soil during installation.

2.4.3 Factors Influencing PVD Efficiency

2.4.3.1 Smear Effect

When prefabricated vertical drains are installed, using a mandrel, significant remoulding of the subsoil occurs in the immediate vicinity of the mandrel. The size of the smear zone is a function of both the mandrel's shape and size. Various researches have proposed models to describe the smear effect –

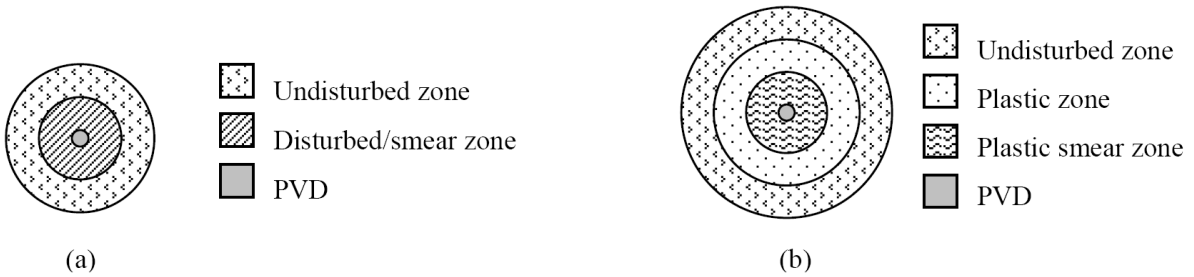

Figure 2.2: Smear zone

Barron (1948) and Hansbo (1981) modelled the smear zone by separating the soil cylinder dewatered by the central drain into two smear zones - Figure 2.2(a).

Onoue et al. (1991) proposed a three-zone smear hypothesis - Figure 2.2(b). The plastic smear zone is located in the immediate vicinity of the vertical drain, where the soil is substantially remoulded as a result of PVD installation (Indraratna et al., 2003). In the plastic zone the permeability is reduced. The soil is unaffected by the installation of the PVD in the undisturbed zone.

Jamiolkowski (1981), Lancellotta (1981) and Hansbo (1987) have all tried to estimate the size of the smear zone. They proposed that the diameter of the smear zone is two to three times the equivalent diameter of the mandrel. Research conducted by Indraratna and Redana (1998) suggested that the smear zone is three to four times the cross-sectional area of the mandrel.

Hansbo (1981), Bergado et al. (1991), Indraratna and Redana (1998) have all verified that the ratio of the coefficient of horizontal permeability (kh) to vertical (kv) can be approximated to unity within the smear zone.

2.4.3.2 Well Resistance

The well resistance of prefabricated vertical drains increases with drain length. Well resistance retards pore water dissipation, which inturn reduces the rate of consolidation. Other factors which increase well resistance include the drain being clogged by fine particles, deterioration of the drain filter and folding of the drain due to lateral movement.

2.4.3.3 Discharge Capacity

The discharge capacity of prefabricated vertical drains could vary from 100 to 800 m3/year based on the filter permeability, core volume or cross-section area, lateral confining pressure, and drain stiffness. As long as the initial discharge capacity of the PVD exceeds 100-150 m3/year, some reduction in discharge capacity due to installation should not seriously influence the consolidation rates. The discharge capacity of most field drains affected by well resistance varies between 40-60 m3/year (Indraratna et al., 2003).

2.4.4 Proposed PVD Models

2.4.4.1 History

In 1948, Barron presented a comprehensive solution to explain the behaviour of radial consolidation by drain wells. He conducted a study on the two extreme cases of free strain and equal strain and concluded that the average consolidation, obtained from both cases, was nearly the same. In his research, Barron also studied the effects of smear and well resistance with respect to the consolidation process of vertical well drains.

Richart (1959) produced design charts to determine the smear effect of prefabricated vertical drains. These charts incorporated the influence of variable void ratio.

Later, Hansbo (1979, 1981) presented a simplified analysis for modelling smear and well resistance.
Nearly two decades later Indraratna and Redana (1997) presented a two-dimensional equivalent plane strain model for the analysis of prefabricated vertical drains.
Recently, Hansbo (1997) again presented another PVD model, which modelled the smear resistance. The difference between this model and his previous model, is that Darcy's Law is not valid.

2.4.4.2 Darcian PVD Models

2.4.4.2.1 Hansbo Model

In 1981 Hansbo presented an approximate solution for vertical drains, based on the equal strain hypothesis, by taking both smear and well resistance into consideration (Indraratna et al., 2003).
Hansbo's solution assumes Darcy's law is valid. He concluded that the average degree of consolidation ($\bar{U}h$) of the soil cylinder with a vertical drain is given by –

$$\overline{U}_h = 1 - \exp\left(-\frac{8c_h t}{\mu D^2}\right) \tag{2.6}$$

$$\mu = \ln\left(\frac{D}{d_s}\right) + \frac{k_h}{k_s}\ln\left(\frac{d_s}{d}\right) - \frac{3}{4} + \pi z(2l - z)\frac{k_h}{q_w} \tag{2.7}$$

If the smear effect is only considered-

$$\mu = \ln\left(\frac{D}{d_s}\right) + \left(\frac{k_h}{k_s}\right)\ln\left(\frac{d_s}{d}\right) - \frac{3}{4} \tag{2.8}$$

If the well resistance is only considered-

$$\mu \approx \ln(D) - \frac{3}{4} + \pi z(2l - z)\frac{k_h}{q_w} \tag{2.9}$$

If the effects of smear and well resistance are ignored-

$$\mu = \ln(D) - \frac{3}{4} \tag{2.10}$$

2.4.4.2.2 Indraratna and Redana Model

In 1997 Indraratna and Redana presented a two-dimensional equivalent plane strain solution for the analysis of embankments with prefabricated vertical drains (PVD).

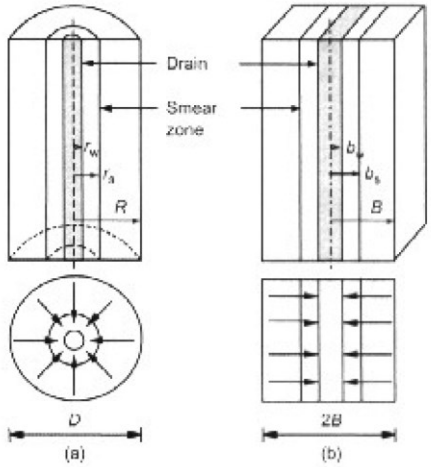

Figure 2.3: Conversion of an axisymmetric unit cell into plane strain (Indraratna et al., 2003)

Indraratna and Redana's model relates the equivalence between the plane strain and axisymmetric analyses. The equivalence between axisymmetric and plane strain conditions can be achieved in three ways (Indraratna et al., 2003):

i. Geometric matching: The spacing of drains is matched while the permeability is kept the same.
ii. Permeability matching: The permeability coefficient is matched, while the spacing is kept the same.
iii. Combine geometric & permeability matching: The plane strain permeability is established for convenient drain spacing.

Indraratna and Redana (1997) converted the vertical drain system (Figure 3(a)) into an equivalent parallel drain element (Figure 3(b)) by changing the soil's permeability coefficient and assuming the width of the plane strain cell was 2B.
The half-width of the drain, bw, and the half-width of the smear zone, bs, are taken to be the same as their axisymmetric radii rw and rs respectively (Indraratna et al., 2003). The average degree of consolidation ($\bar{U}hp$) under plain strain conditions is given by -

$$\bar{U}_{hp} = 1 - \frac{\bar{u}}{u_o} = 1 - \exp\left(-\frac{8T_{hp}}{\mu_p}\right) \qquad (2.11)$$

$$\mu_p = \left[\alpha + (\beta)\frac{k_{hp}}{k'_{hp}} + (\theta)\left(2lz - z^2\right)\right] \qquad (2.12)$$

In the above formula the geometry terms α and β and flow parameter θ are –

$$\alpha = \frac{2}{3} - \frac{2b_s}{B}\left(1 - \frac{b_s}{B} + \frac{b_s^2}{3B^2}\right) \tag{2.13}$$

$$\beta = \frac{1}{B^2}(b_s - b_w)^2 + \frac{b_s}{3B^3}\left(3b_w^2 - b_s^2\right) \tag{2.14}$$

$$\theta = \frac{2k_{hp}^2}{k'_{hp} q_z B}\left(1 - \frac{b_w}{B}\right) \tag{2.15}$$

For a certain stress level and time interval, the degree of consolidation for axisymmetric ($\bar{U}h$) and equivalent plane strain ($\bar{U}hp$) conditions can be made equal (Indraratna et al., 2003). The time factor ratio can be determined when equation (2.11) and equation (2.16) are combined with Hansbo's equation (2.6) –

$$\overline{U}_h = \overline{U}_{hp} \tag{2.16}$$

$$\frac{T_{hp}}{T_h} = \frac{k_{hp}}{k_h}\frac{R^2}{B^2} = \frac{\mu_p}{\mu} \tag{2.17}$$

For simplicity assume R = B, giving the following relationship between K_{hp} and K'_{hp} –

$$k_{hp} = \frac{k_h\left[\alpha + (\beta)\frac{k_{hp}}{k'_{hp}} + (\theta)\left(2lz - z^2\right)\right]}{\left[\ln\left(\frac{D}{d_s}\right) + \left(\frac{k_h}{k_s}\right)\ln\left(\frac{d_s}{d}\right) - \frac{3}{4} + \pi\left(2lz - z^2\right)\frac{k_h}{q_w}\right]} \tag{2.18}$$

If the well resistance is ignored the smear effect can be modelled by –

$$\frac{k'_{hp}}{k_{hp}} = \frac{\beta}{\frac{k_{hp}}{k_h}\left[\ln\left(\frac{D}{d_s}\right) + \left(\frac{k_h}{k_s}\right)\ln\left(\frac{d_s}{d}\right) - \frac{3}{4}\right] - \alpha} \tag{2.19}$$

If both well resistance and smear are ignored, Hird et al. (1992) proposed the following expression -

$$\frac{k_{hp}}{k_h} = \frac{0.67}{\left[\ln\left(\frac{D}{d_s}\right) - \frac{3}{4}\right]} \tag{2.20}$$

2.4.4.3 Proposed Non-Darcian PVD Model

Research conducted by Silfverberg (1947), Hansbo (1960), Miller & Low (1963), Dubin & Moulin (1986) into the permeability of clay samples, revealed that the pore water flow (v) caused by a hydraulic gradient (i) may deviate from Darcy's law. Silfverberg and Miller & Low came to the conclusion that there is a threshold gradient (io) below which no flow (v) will develop, yielding –

$v = k(i - i_o)$ (2.21)

In 1960 S. Hansbo proposed an alternative expression to determine the flow velocity (v) –

$v = ki^n$ when $i \leq i_1$ (2.22)

$v = k(i - i_o)$ when $i \geq i1$ where $i_1 = i_o n/(n-1)$ (2.23)

In his opinion the i1 term, in the above equation, represents the hydraulic gradient required to overcome the maximum binding energy of mobile pore water.

From his research into the effects of Non-Darcian flow, Hansbo developed an alternative consolidation equation to model prefabricated vertical drain –

$$t = \frac{\alpha D^2}{\lambda}\left(\frac{D\gamma_w}{u_o}\right)^{n-1}\left(\frac{1}{(1-\overline{U}_h)^{n-1}} - 1\right) \qquad (2.24)$$

$$\alpha = \frac{n^{2n}\beta^n}{4(n-1)^{n+1}} \qquad (2.25)$$

$$\beta = \frac{1}{3n-1} - \frac{n-1}{n(3n-1)(5n-1)} - \frac{(n-1)^2}{2n^2(5n-1)(7n-1)} + \frac{1}{2n}\left[\left(\frac{k_h}{k_s} - 1\right)\left(\frac{D}{d_s}\right)^{-(1-(1/n))} - \frac{k_h}{k_s}\left(\frac{D}{d}\right)^{-(1-(1/n))}\right] \qquad (2.26)$$

Equation (2.24) can be used to determine the time required to reach a certain average degree of consolidation. This equation also includes the negative effect of smear on the consolidation process (Hansbo, 1997).

When n = 1, equation (2.24) will yield the same result as Hansbo's consolidation equation (2.6) provided that the well resistance is ignored and $\lambda = Ch$.

The theoretical results obtained from Hansbo's equation were verified by extensive full-scale field tests. The best agreement between Hansbo's solution and the field data was achieved when n = 1.5. Thus, equation (2.24) now becomes –

$$\overline{U}_h = 1 - \left[1 + \frac{\lambda t}{\alpha D^2}\left(\frac{u_o}{D\gamma_w}\right)^{1/2}\right]^{-2} \quad (2.27)$$

$$\alpha = 4.77\beta\sqrt{\beta} \quad (2.28)$$

$$\beta = 0.270 + \frac{1}{3}\left[\left(\frac{k_h}{k_s} - 1\right)\left(\frac{D}{d_s}\right)^{-1/3} - \frac{k_h}{k_s}\left(\frac{D}{d}\right)^{-1/3}\right] \quad (2.29)$$

2.4.4.4 Correlation between Darcian and Non-Darcian PVD Models

To determine the adequacy of both Hansbo's Darcian and Non-Darcian PVD models, these models were tested on three trial embankment - Skå-Edeby (located in Sweden), Porto Tolle and Bangkok. These sites were selected because they represent different soil conditions and are located in different parts of the world.

For all three trial embankments, there was a better correlation between the field data and the output obtained from the Non-Darcian equation (2.27). Thus equation (2.27) has a better overall representation of the field conditions than Darcian PVD model i.e. equation (2.6).

2.4.4.5 Corrections for Band Drains

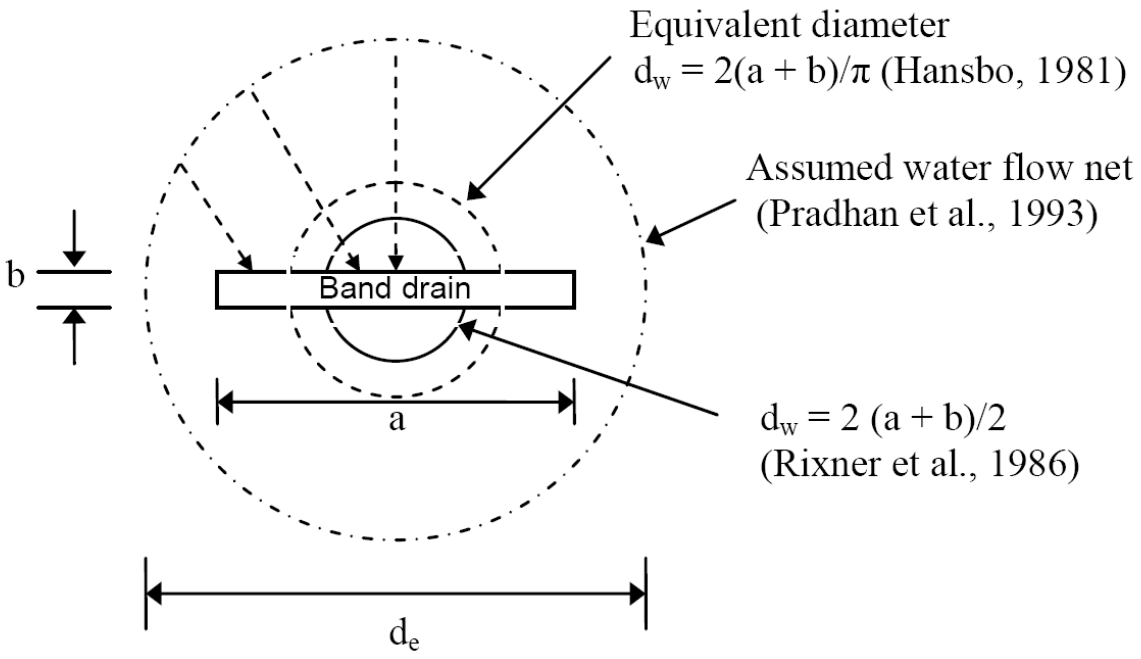

Figure 2.4: Equivalent diameter of band-shaped vertical drains

The conventional consolidation theory of vertical drains assumes the drains to have a circular cross-section. When analysing band-shaped drains, the cross-section should be transformed to an equivalent circle such that the equivalent circular drain has the same theoretical radial drainage capacity as the band-shaped drain (Indraratna et al., 2003).

In 1981 Hansbo proposed the following expression to determine the equivalent diameter (d_w) for a prefabricated band-shaped drain –

$$d_w = \frac{2(a+b)}{\pi} \quad (2.30)$$

In 1986 Rixner et al. suggested a simpler expression to determine the equivalent diameter (d_w) for a prefabricated band-shaped drain –

$$d = \frac{a+b}{2} \quad (2.31)$$

This formula takes into consideration the drain shape and the effective drainage area and is an average of the drain thickness and width. In 1993 Pradhan et al. suggested that the flow net around the soil cylinder of diameter (d_e) should be used in the estimation of the equivalent diameter of the band-shaped drain. The mean square distance of the flow net is given by –

$$\bar{s}^{-2} = \frac{1}{4}d_e^2 + \frac{1}{12}a^2 - \frac{2a}{\pi^2}d_e \quad (2.32)$$

And the equivalent drain diameter (d_w) is given by –

$$d_w = d_e - 2\sqrt{\left(\bar{s}^{-2}\right)} + b \quad (2.33)$$

2.4.4.5.2 Influence Zone

The rate of consolidation is affected by the prefabricated vertical drains spacing pattern. Vertical drains are generally spaced in either a square or triangular pattern. Indraratna et al. (2003) presented equations to determine the influence zone of PVDs spaced in a square and triangular pattern. The PVD influence zone is the zone in which pore water can dissipate into the drain. The diameter of the influence zone (D) for drains installed in a square pattern is given by –

D = 1.13S (2.34)

The diameter of the influence zone (D) for drains installed in a triangular pattern is given by –

D = 1.05S (2.35)

Where S = Drain spacing

Installing drains in a square pattern is much easier than installing drains in a triangular pattern. The advantage of installing a triangular layout is that it provides a more uniform rate of consolidation between drains.

2.5 Stone Columns

Another method of accelerating the consolidation rate of soft marine clays is to install stone columns. Stone columns are extensively used to improve the bearing capacity of poor ground

and reduce settlement of structures built on them (Lee et al., 1998). Stone columns consist of crushed rock, generally have a diameter which ranges between 0.6 to 1.0m and may be as long as 20m (Mitchell, 1981). Stone columns are normally installed in either a square or triangular pattern; with centre to centre spacing of 1.5 to 3.5m (Mitchell, 1981).

2.5.1 Stone Column Installation

The replacement and/or displacement method is commonly used to install stone columns. The replacement method involves replacing the in-situ soil with stone columns. A vibratory probe (vibroflot), accompanied by a water jet, is used to create the holes for the columns. This technique is suitable when the ground water level is high and the in-situ soil is relatively soft (Lee et al., 1998). The displacement method is utilised when the water table is low and the in-situ soil is firm. It involves using a vibratory probe, which uses compressed air, to displace the natural soil laterally.

2.5.2 Benefits

There are numerous benefits of installing stone columns, which include –

i. Substantial increase in the shear strength of the original ground (Cooper et al., 1999).
ii. Enhanced drainage of excess pore water, as stone columns have high permeability by comparison with clay (Muir Wood et al., 2000).
iii. Higher frictional strength and stiffness than soft clay i.e. they behave more like a pile foundation.
iv. Resist shear in the horizontal and inclined directions (Mitchell, 1981).

Stone columns are also very effective in accelerating the rate of consolidation, if the horizontal coefficient of consolidation (c_h) is much greater than the vertical (c_v). This is because the drainage path in the radial direction is considerably reduced.

2.5.3 Proposed Stone Column Models

The degree of consolidation of a soil cylinder with stone columns can be determined using Barron's classical consolidation formula or by a simple one-dimensional analysis.

2.5.3.1 Barron Model

In 1947 Barron presented an expression to determine the degree of consolidation (U) of a cylindrical block of clay surrounding vertical drains/stone columns –

$$U = 1 - \exp\left(-\frac{2T_r}{F}\right) \tag{2.36}$$

$$F = \frac{\ln \chi}{1-\chi^2} - \frac{3-\chi^{-2}}{4} \tag{2.37}$$

2.5.3.2 One Dimensional Analysis

Wood et al. (2000) proposed a simple one-dimensional analysis which can be used to estimate the degree of consolidation (U) in a cylindrical soil region around a vertical drain (Muir Wood et al., 2000).

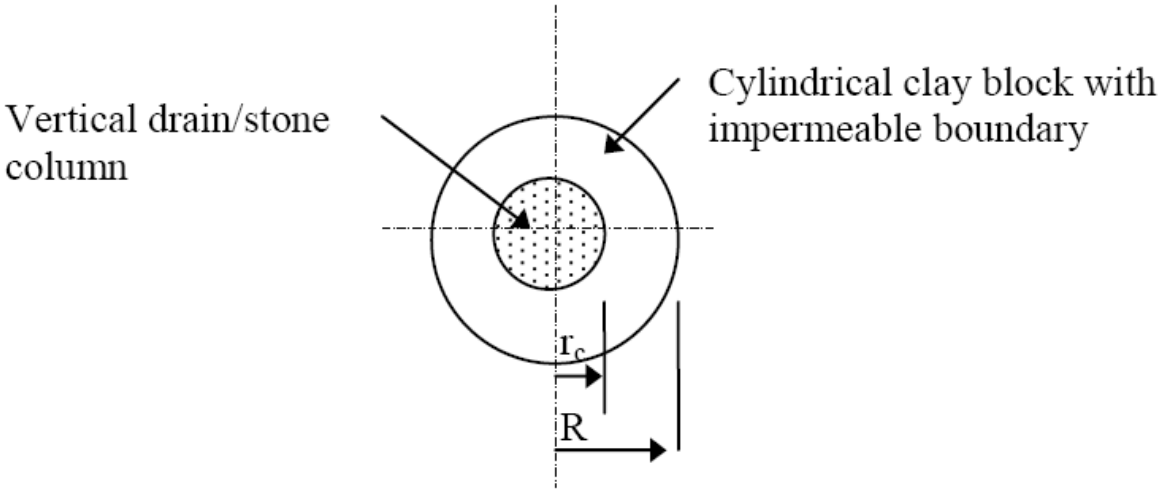

Figure 2.5: Sectional view of vertical drain

To determine the degree of consolidation, the radial variation in pore pressure must first be established –

$$u = \frac{\gamma_w \dot{\varepsilon}}{4k_h}\left[2R^2 \ln\left(\frac{r}{r_c}\right) - (r^2 - r_c^2)\right] \qquad (2.38)$$

Integrating equation (2.38) over the radius will give an estimation of the average pore pressure (u_{av}). An average degree of consolidation (U_{av}) can then be obtained when the average pore pressure is compared with –

$$U_{av} = 1 - \frac{F}{2T_r} \qquad (2.39)$$

2.5.4 Engineering Behaviour of Composite Ground

2.5.4.1 Basic Relationship

In 1996, Bergado et al. presented a theory to determine the settlement and stability of ground reinforced with stone columns. The theory is based on the stress concentration in the granular pile. Figure 2.6 illustrates a diagram of the composite ground -

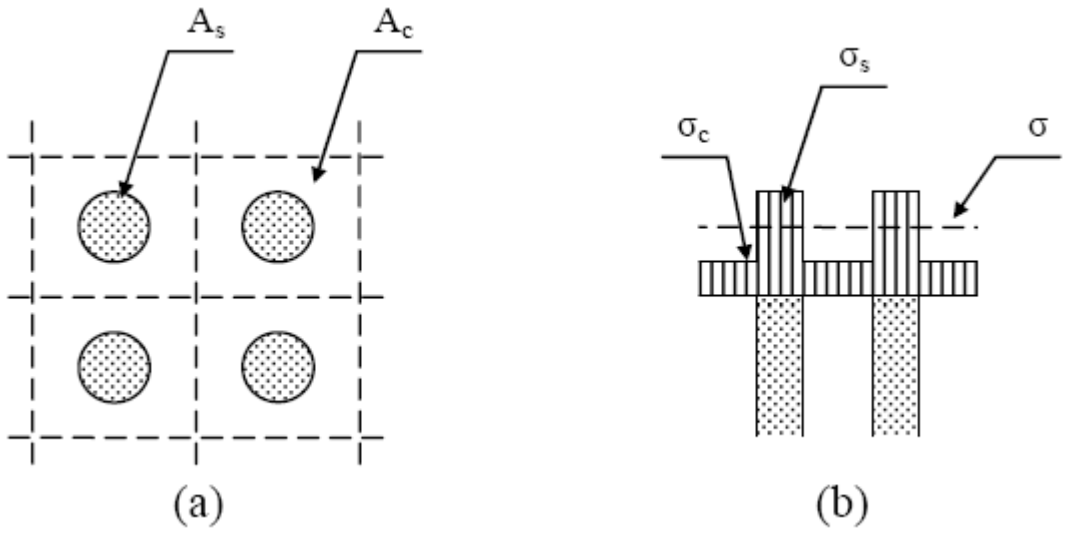

Figure 2.6: Diagram of composite ground (Bergado et al., 1996)

Each stone column is separated into its own unit cell - Figure 2.6(a). The unit cell is defined as the cylinder with an influence zone diameter (D) enclosing the tributary soil and one stone column. The area replacement ratio is the ratio of the granular pile area (As) over the whole area of the equivalent cylindrical unit within the unit cell (Bergado et al., 1996) -

$$a_s = \frac{A_s}{A_s + A_c} \tag{2.40}$$

This ratio can also be expressed in terms of the stone column diameter (Ds) and spacing (S). The area replacement ratio for stone columns installed in a square and equilateral triangular pattern is respectively -

$$a_s = \frac{\pi}{4}\left(\frac{D_s}{S}\right)^2 \tag{2.41}$$

$$a_s = \frac{\pi}{2\sqrt{3}}\left(\frac{D_s}{S}\right)^2 \tag{2.42}$$

The distribution of the stress in the stone column (σ_s), clayey ground (σ_c) and average stress (σ) is illustrated in Figure 2.6(b). Studies have shown that when ground reinforced with stone columns is loaded, stress concentrations develop in the column accompanied by a reduction in stress in the surrounding clayey ground. This can be explained by the fact that, when loaded, the vertical settlement of the stone column and the surrounding soil is approximately the same, causing the occurrence of stress concentration in the column which is stiffer than the surrounding cohesive soil (Bergado et al., 1996).

A stress concentration factor (n) is used to express the distribution of vertical stress within the unit cell -

$$n = \frac{\sigma_s}{\sigma_c} \tag{2.43}$$

The relative stiffness of the stone column and surrounding soil is affected by the magnitude of the stress concentration. The average stress (σ) over the unit cell area is given by -

$$\sigma = \sigma_s a_s + \sigma_c (1 - a_s) \tag{2.44}$$

The stress in the stone column (σ_s) and stress in the surrounding clayey ground (σ_c) is respectively -

$$\sigma_s = \frac{n\sigma}{[1 + (n-1)a_s]} = \mu_s \sigma \tag{2.45}$$

$$\sigma_c = \frac{\sigma}{[1 + (n-1)a_s]} = \mu_c \sigma \tag{2.46}$$

2.5.4.2 Settlement

Most of the approaches in estimating settlement of ground reinforced with stone columns assume an infinitely wide, loaded area reinforced with granular piles having a constant diameter and spacing (Bergado et al., 1996).

In 1996, Bergado et al. presented the following expression to determine the settlement (S_t) of ground reinforced with stone columns –

$$S_t = m_v(\mu_c \sigma)H \tag{2.47}$$

2.5.4.3 Slope Stability

Installing stone columns, beneath a road embankment constructed on soft marine clay can increase its overall stability. The three most commonly used methods of analysing the stability of composite ground are the profile, average shear strength and lumped parameter method.

2.5.4.3.1 Profile Method

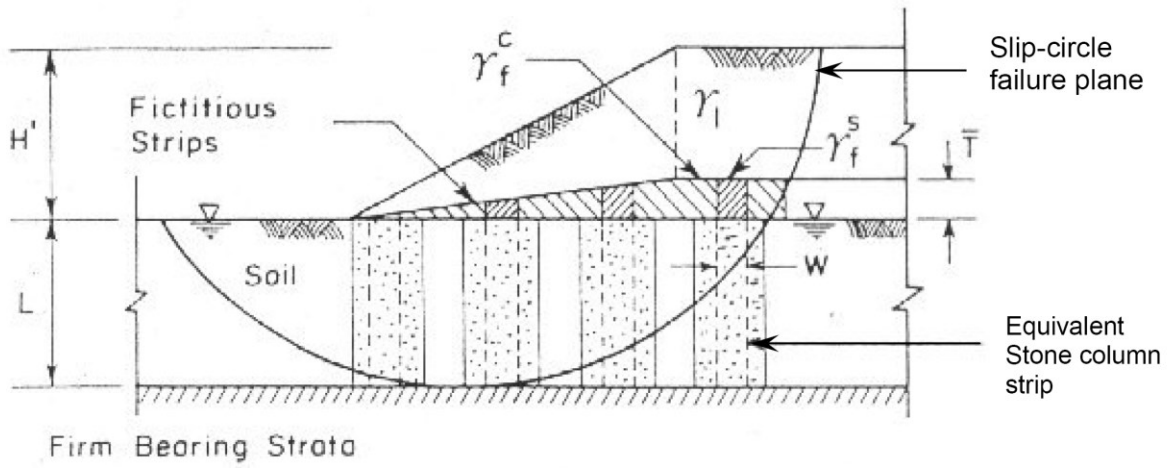

Figure 2.7: Granular pile strip idealization and fictitious soil layer for slope stability analysis (Bergado et al., 1996)

The profile method involves converting each row of the stone columns into an equivalent continuous strip of width (w) - Figure 2.7. The actual geometry and material properties are then used to analyse each strip of cohesion less and cohesive soils.

In order to produce an economical design, the stress concentrations which develop in the piles must be taken into consideration (Bergado et al., 1996). The stress concentration in the stone column increases the magnitude resisting shear force acting along the slip-circle failure plane. Thin fictitious strips of soil are placed above the in-situ soil and stone columns at the embankment interface to model the effect of the stress concentration in the column. The weights of the fictitious soil strips placed above the stone columns are relatively large to cause the desired stress concentration. The weight of the clayey ground and stone column fictitious strip is respectively –

$$\gamma_f^c = \frac{(\mu_c - 1)\gamma_1 H'}{\bar{T}} \qquad (2.48)$$

$$\gamma_f^s = \frac{(\mu_s - 1)\gamma_1 H'}{\bar{T}} \qquad (2.49)$$

It should be noted that the fictitious strips placed above the in-situ soil and granular piles have no shear strength (Bergado et al., 1996). Also limits must be imposed on the grid size of slip-circle centres and radius, to ensure that the critical slip-circle isn't affected by the fictitious interface layer.

2.5.4.3.2 Average Shear Strength Method

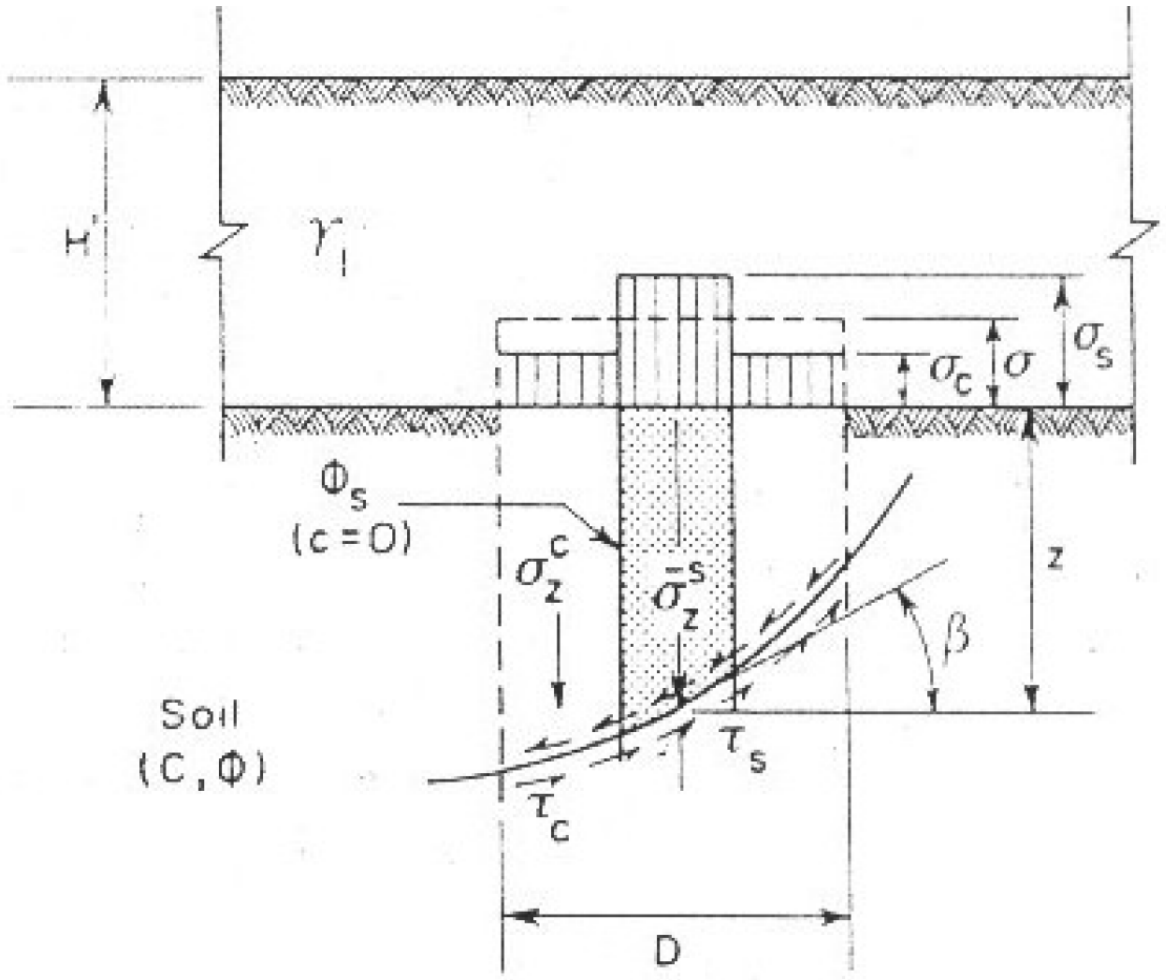

Figure 2.8: Average stress method of stability analysis (Bergado et al., 1996)

The average shear strength method is widely used in stability analysis for sand compaction piles (Bergado et al., 1996). This technique considers the weighted average of the material properties inside the unit cell; which is appealing for hand calculations.

The distribution of stress within the unit cell is illustrated when referring to Figure 2.8. The effective stresses in the stone column and total stress in the surrounding soil is respectively -

$$\sigma_z^s = \gamma_s z + \sigma\mu_s \tag{2.50}$$

$$\sigma_z^c = \gamma_c z + \sigma\mu_c \tag{2.51}$$

The shear strength of the stone column and the surrounding soil is respectively determined by

$$\tau_s = \left(\sigma_z^s \cos^2\beta\right)\tan\varphi_s \tag{2.52}$$

$$\tau_c = c + \left(\sigma_z^c \cos^2\beta\right)\tan\varphi_c \tag{2.53}$$

The weighted average shear strength (τ) and weight average unit weight (γ_{avg}) within the unit cell is given by –

$$\tau = (1 - a_s)\tau_c + a_s\tau_s \quad (2.54)$$

$$\gamma_{avg} = \gamma_s a_s + \gamma_c a_c \quad (2.55)$$

The shear strength parameters for use in this technique are –

$$c_{avg} = c(a_s) \quad (2.56)$$

$$(\tan\varphi)_{avg} = \frac{\gamma_s a_s \tan\varphi_s + \gamma_c a_c \tan\varphi_c}{\gamma_{avg}} \quad (2.57)$$

2.5.4.3.3 Lumped Parameter Method

The lumped parameter technique is used to establish the factor of safety (SF) of the embankment and is given by the following expression –

$$SF = \frac{(RM + \Delta RM)}{(DM + \Delta DM)} \quad (2.58)$$

The resisting moment (RM) and driving moment (DM) are first calculated for the condition of no stone columns. These terms are then recalculated considering the effect of the stone columns.

2.5.5 Factors Influencing Stone Column Efficiency

2.5.5.1 Deformations

In 1974 Hughes and Withers studied the behaviour of single stone columns. They used laboratory radiography to observe the deformations occurring in and around a column of sand loaded within a cylindrical chamber containing clay (Muir Wood et al., 2000). Hughes and Withers concluded that stone column bulging deformation occurs within four column diameters, measured from the column's surface, and the capacity of stone column can be assumed by observing the behaviour of bulging stone columns as they expand radially into the surrounding clay. In their research of stone columns, Muir Wood et al. (2000) established that the length of a stone column can reduce the mechanism of deformation to a point. Beyond this point, increasing the column length gives no further advantage.

2.5.5.2 Failure Patterns

Muir Wood et al. (2000) proposed the following four failure modes of stone columns -

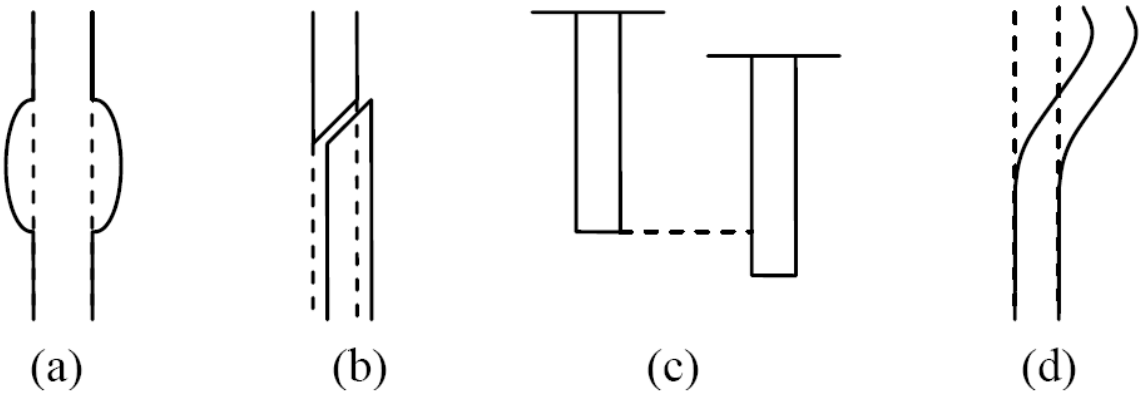

Stone columns can fail by bulging, if it is not prevented from expanding radially by adjacent columns – Figure 2.9(a). If a column has little lateral restraint and is subjected to high loads, it may fail by a diagonal shear plane – Figure 2.9(b). Stone columns can fail by penetration through an underlying soft clay layer – Figure 2.9(c). A slender stone column can fail if it's laterally loaded – Figure 2.9(d).

2.5.5.3 Smear Effect/Well Resistance

Stone columns are also affected by smear and well resistance, in a similar manner as are prefabricated vertical drains.

2.5.6 Case Study: Coombabah Creek Embankment

In 1995 a trial embankment was built by the Queensland Department of Main Roads at Coombabah Creek. The embankment was constructed to asses the effectiveness of stone columns for both settlement reduction and acceleration (Wijeyakulasuriya et al., 1999). This embankment was constructed on a soft marine clay stratum. The embankment was divided into three sections, two sections had stone columns (m 1 =) spaced at 2m and 3m, and the other section contained no ground improvement. The stone columns were installed using the replacement method. The lack of a weathered crust, at the Coombabah Creek site, is expected to offer little passive resistance against lateral bulging of the stone columns - Figure 2.9(a). This will also minimise the column's load capacity. Wijeyakulasuriya et al. concluded that the use of stone columns did not indicate real gains either in terms of settlement or consolidation times. Also the results obtained from the different column spacings were comparable. They postulated that such stone column performances are due to disturbances caused to sensitive soft clays during installation (Wijeyakulasuriya et al., 1999).

2.6 Deep Mixing Methods

The deep mixing method is a ground improvement technique used to improve the overall performance of compressible soil masses under relatively lightly loaded structures, such as road embankments (Bruce, 2001). Cementitious materials are commonly used in deep mixing. The material is introduced and blended into the soil through hollow, rotated shafts equipped with cutting tools, and mixing paddles that extend for various distances above the tip (Bruce, 2001). The binder material is then injected into the soil in either a wet or dry form. Generally the treated ground has higher strength, but, lower compressibility and permeability than the virgin soil.

2.7 Conclusion

In South East Queensland many road embankments are constructed on soft sensitive marine clays of low strength and high compressibility. Structures built on these sites are subject to damage from differential settlement. Employing ground improvement techniques is one way of overcoming structure distress. Pre-loading in combination with prefabricated vertical drains and stone columns and deep mixing methods are all examples of soil improvement techniques. These methods are used to improve the properties of the foundation material. As the population of South East Queensland increases, the advantages of ground improvement techniques need to be draw upon. Once thought unsuitable land can be reclaimed and used for road construction.

CHAPTER 3: SOIL CHARACTERISTICS

3.0 Introduction

Contained within chapter 3 are the soil characteristics of the site where the trial embankment was built. Included in this section are the in-situ conditions before the embankment was constructed and the subsequent conditions after the embankment was built. From the laboratory results, the one dimensional settlement of the embankment was predicted. The vertical settlement (both surface and sub-surface), horizontal settlement profile, lateral displacement and excess pore pressure plots, determined from the in-situ field equipment, are provided.

3.1 General

The Coombabah Creek trial embankment is located in a marine environment. It passes through a low lying wetland reserve. The soil found here is predominately soft organic marine clay. Before the trial embankment was constructed, numerous bore holes were drilled and undisturbed soil samples taken, to assess the soil characteristics. These characteristic were then utilised in the design and construction of the trial embankment. During the construction of the embankment, field instrumentation was installed to monitor the performance of the embankment, both during and after it was built.

3.2 Longitudinal soil profile

The trial embankment was built along the deepest section of the very soft to soft organic clay layer, which extended to a maximum depth of 13.5m. Underlying this layer is a moderately dense to dense sandy sediment strata. On either side of these strata are stiff-hard clay/silty clay. The longitudinal profile of the soil stratum is displayed on the proceeding page.

3.3 Embankment geometry and construction schedule

One trial embankment was constructed along the Gold Coast Highway. This embankment was divided into three sections – section (1) contained no ground improvement, section (2) had stone columns at 2m spacing and section (3) had stone columns at 3m spacing. The stone columns had a diameter of 1m and were 16m long. The Coombabah Creek embankment was constructed in two stages. Stage one construction was 2m high, while stage two constructions varied for each section. Beneath the embankment, Geogrid was placed to reinforce the embankment. The geometry of the trial embankment is illustrated on the page after the longitudinal soil profile.

LONGITUDINAL PROFILE

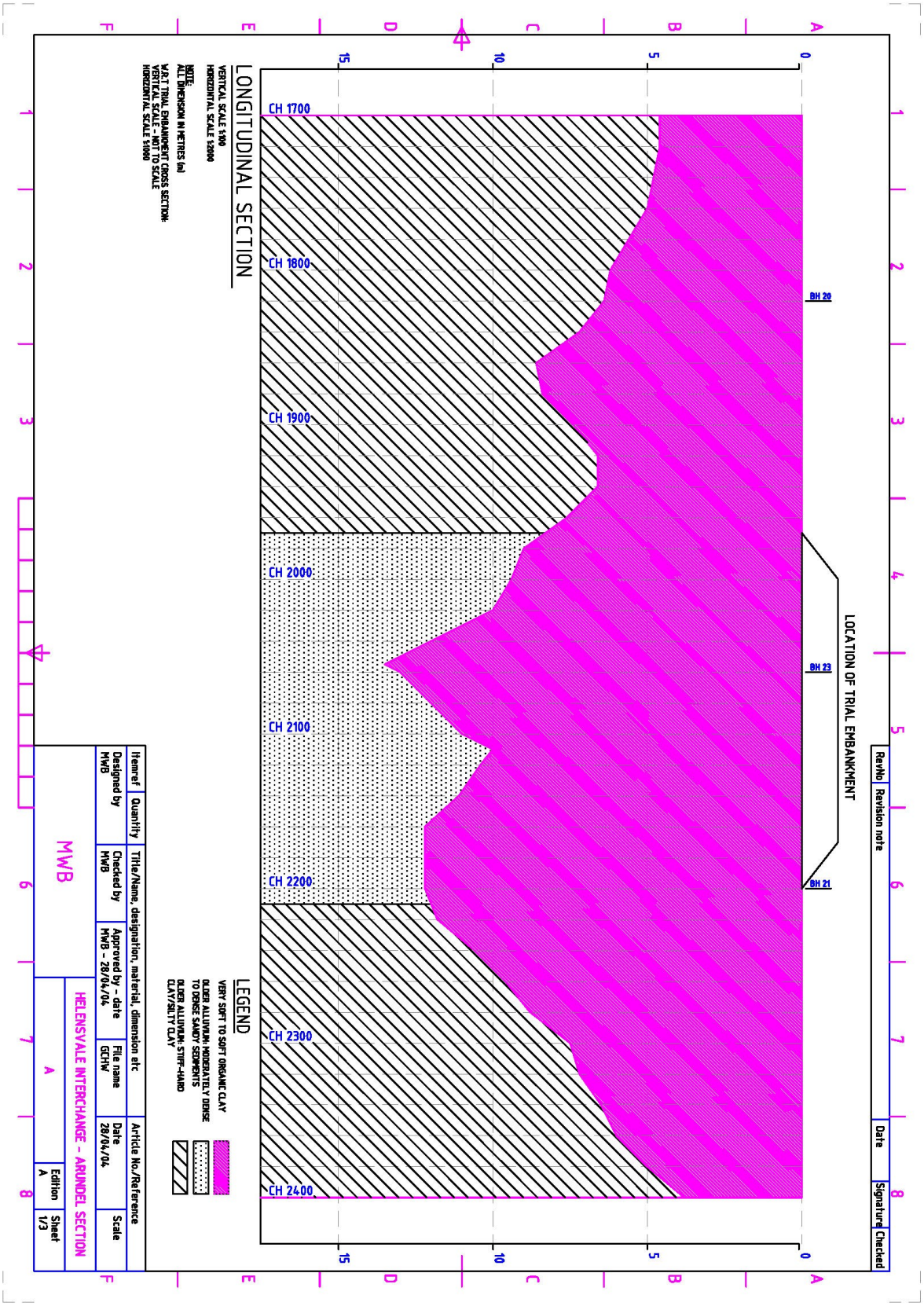

TRIAL EMBANKMENT GEOMETRY

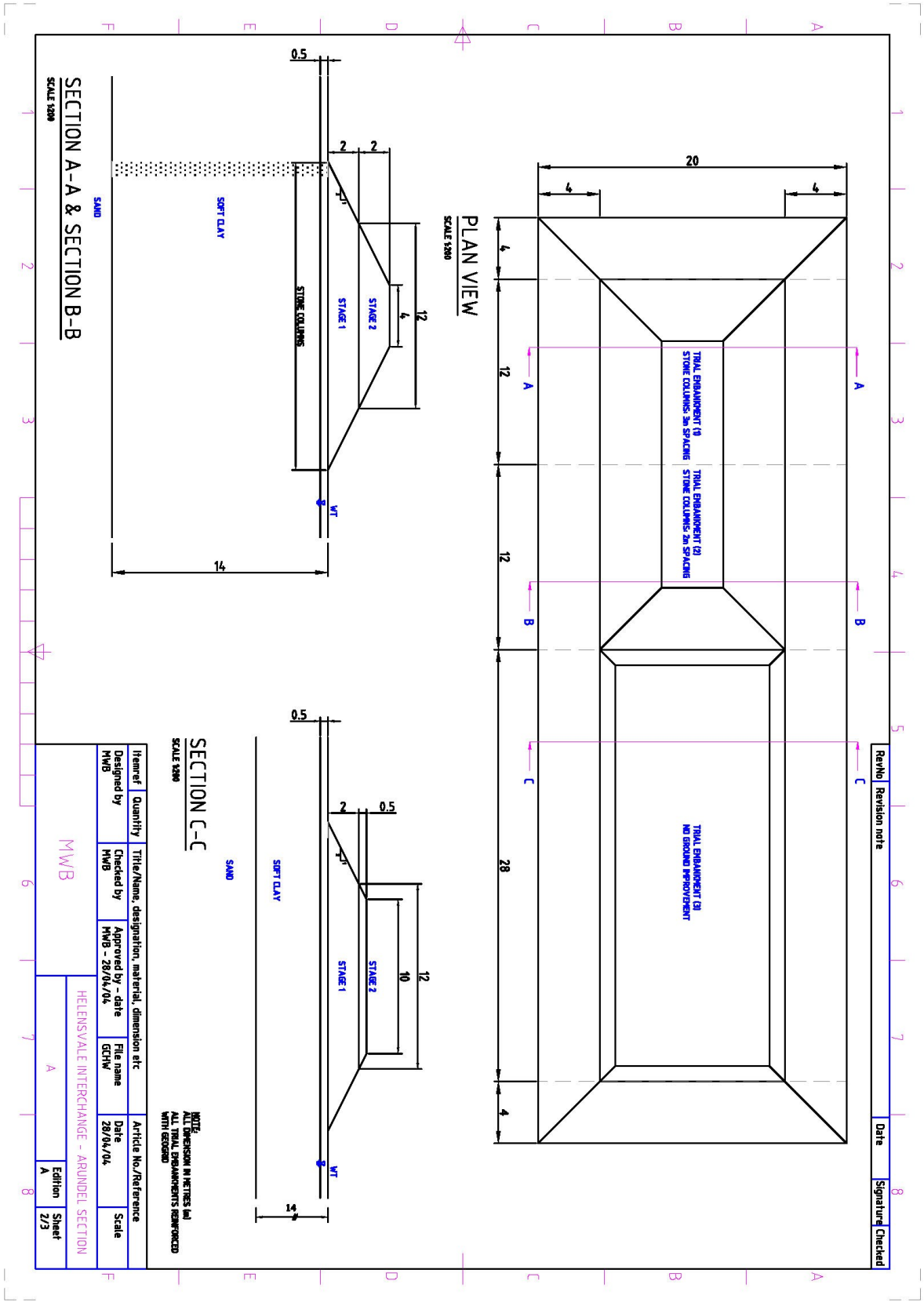

The exact construction schedule of the trial embankment is unknown from the Queensland Department of Main Roads (QDMR) reports. Knowledge from the Principal Geotechnical Testing Officer at QDMR suggests that it took 35 days to construct each stage and there was a period of 100 days (consolidation period) between each stage.

The exact construction schedule of the trial embankment is unknown from the Queensland Department of Main Roads (QDMR) reports. Knowledge from the Principal Geotechnical Testing Officer at QDMR suggests that it took 35 days to construct each stage and there was a period of 100 days (consolidation period) between each stage.

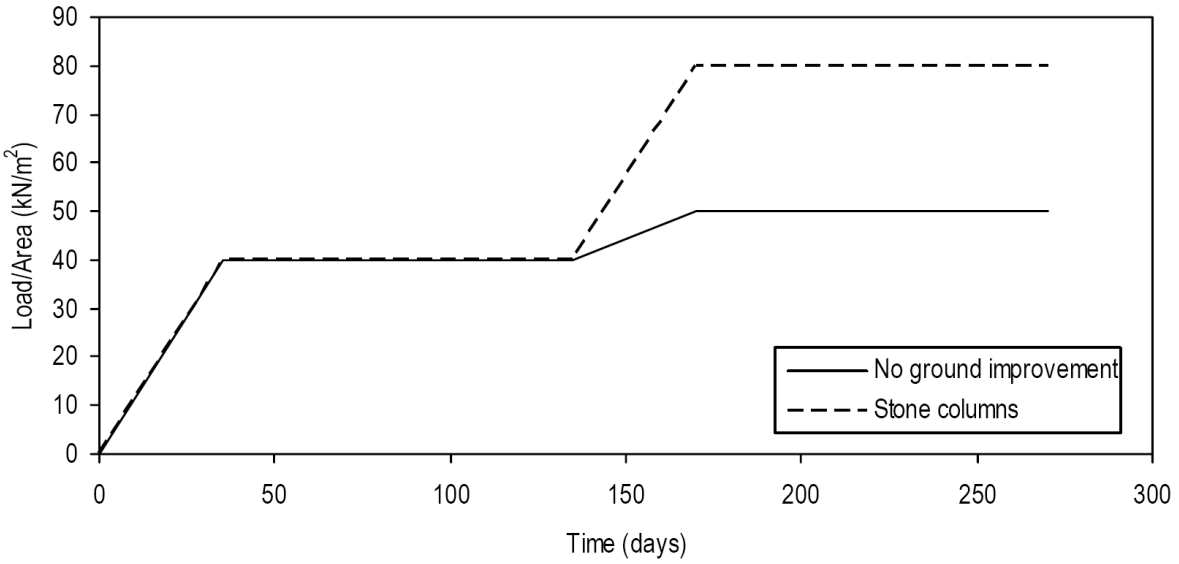

Figure 3.1: Construction schedule

3.4 In-situ field conditions

Numerous bore holes were drilled along the site where the trial embankment was built. From the bore holes, undistributed soil samples were taken, at various depths, to determine the nature of the soil stratum. Laboratory tests were used to establish the wet density (γ_{wet}) of the soft organic clay – Figure 3.2(a). The undrained shear strength (Su) of the soft clay was also determined at various depths – Figure 3.2(b).

Once the wet density (γ_{wet}) is known the total vertical stress (σ_v), pore pressure (u) and effective vertical stress (σ_v ') can then be calculated for the condition before the embankment is constructed. The variations of these parameters with depth are shown in Figure 3.2(c), Figure 3.2(d) and Figure 3.2(e) respectively. The raw data used to produce these plots is displayed in Table 3.1. The coloured figures in Table 3.1 are obtained from the stated bore holes. The uncoloured figures are the assumed distribution.

Table 3.1: Insitu field conditions

Depth (m)	γ_{wet} (kN/m^3)	Su (kPa)	σ_v (kN/m^2)	u (kN/m^2)	σ'_v (kN/m^2)	BH
0.0	14.3	7.50	0.00	0.00	0.00	
0.5	14.3	8.00	7.15	0.00	7.15	BH20
1.0	14.3	8.50	14.30	4.90	9.40	BH20
1.5	14.3	9.00	21.45	9.81	11.64	
2.0	14.3	10.00	28.60	14.71	13.89	
2.5	14.3	10.50	35.75	19.61	16.14	BH20
3.0	14.3	11.00	42.90	24.52	18.38	BH20
3.5	14.4	12.00	50.40	29.42	20.98	
4.0	14.4	12.50	57.60	34.32	23.28	
4.5	14.5	13.00	65.25	39.23	26.02	BH21
5.0	14.5	14.00	72.50	44.13	28.37	BH21
5.5	14.7	14.50	80.85	49.04	31.82	
6.0	14.7	15.00	88.20	53.94	34.26	
6.5	14.9	16.00	96.85	58.84	38.01	
7.0	14.9	16.50	104.30	63.75	40.55	
7.5	15.1	17.00	113.25	68.65	44.60	
8.0	15.1	17.50	120.80	73.55	47.25	
8.5	15.3	18.00	130.05	78.46	51.59	BH21
9.0	15.3	18.50	137.70	83.36	54.34	BH21
9.5	15.5	19.00	147.25	88.26	58.99	
10.0	15.6	20.00	156.00	93.17	62.83	
10.5	15.9	21.00	166.95	98.07	68.88	
11.0	15.9	21.50	174.90	102.97	71.93	
11.5	16.1	22.00	185.15	107.88	77.27	BH23
12.0	16.1	22.50	193.20	112.78	80.42	BH23
12.5	16.3	23.00	203.75	117.68	86.07	
13.0	16.3	24.00	211.90	122.59	89.31	
13.5	16.5	24.50	222.75	127.49	95.26	
14.0	16.5	25.00	231.00	132.39	98.61	

Oedometer consolidation tests were also undertaken, in the laboratory, to assess the compressibility characteristics of the soft organic clay. Figure 3.3 illustrates the compression curves for five different soil samples taken from bore holes located along the Gold Coast highway site at Coombabah Creek.

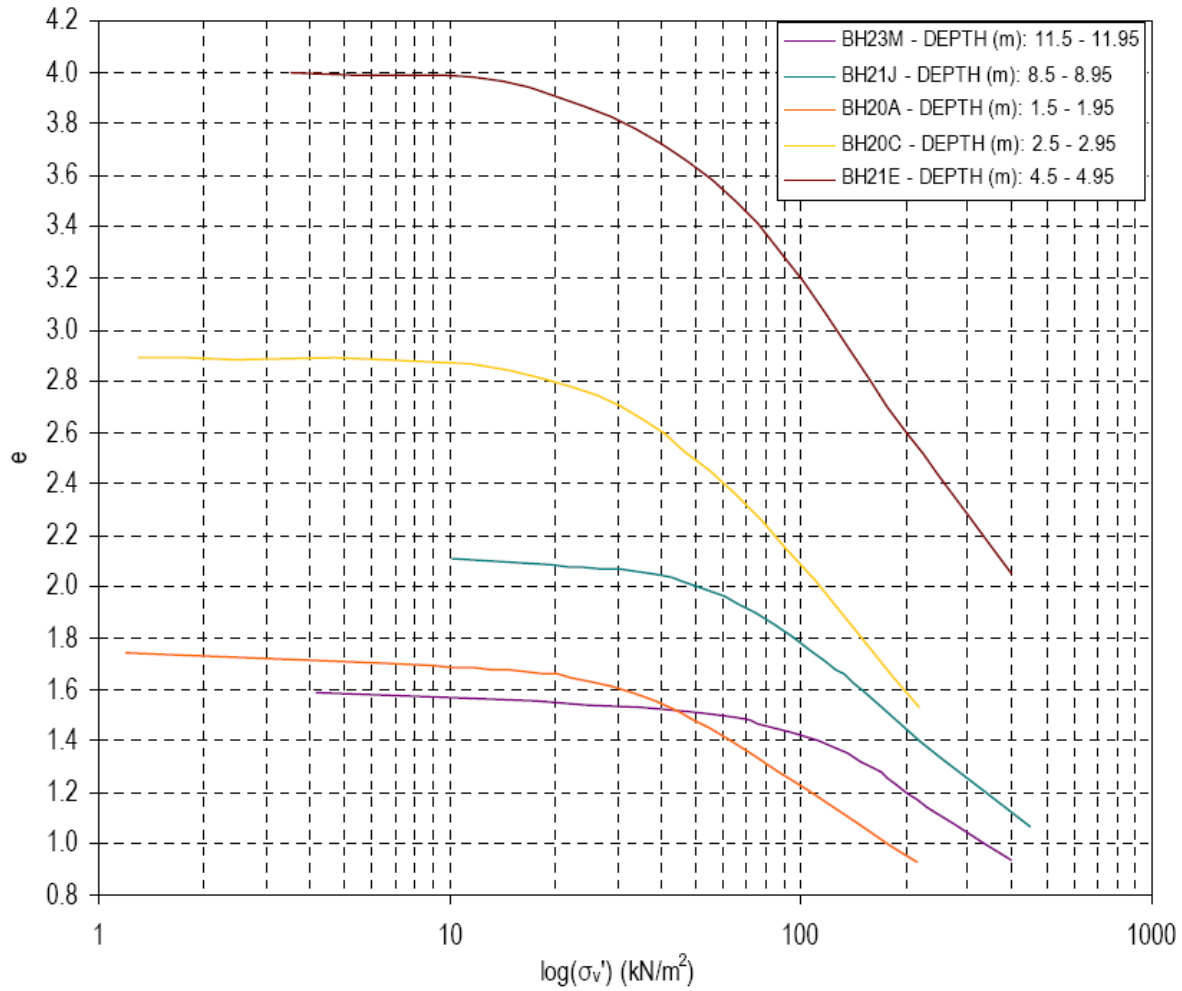

Figure 3.3: Consolidation curves at various depths

From these curves the coefficient of volume decrease (m_v) and coefficient of consolidation (c_v) can be determined. In Appendix A the coefficient of consolidation (c_v) for the bore holes in Figure 3.3 is shown.

3.5 Conditions after embankment construction

The weight of the trial embankment causes an increase in the vertical stress in the soft clay layer. This increase in stress and/or incremental stress ($\Delta\sigma_v$) decreases with depth below the embankment. The following expression was used to determine the vertical stress in a semi-finite mass due to embankment loading –

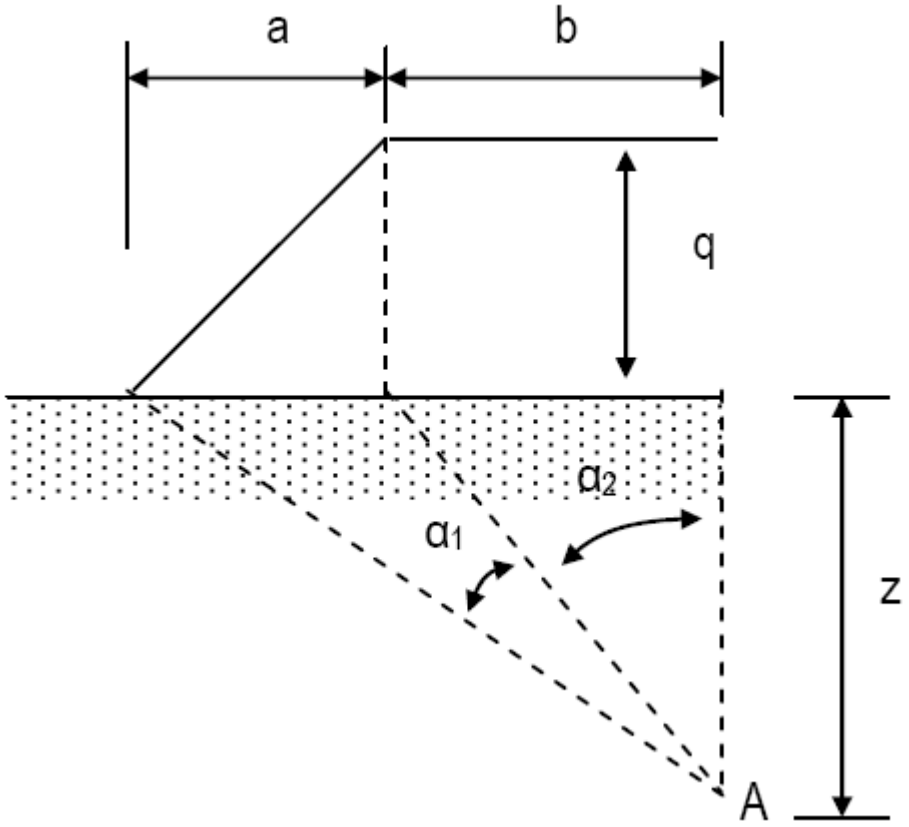

Figure 3.7: Vertical stress due to embankment loading

Incremental stress at point A due to embankment loading shown in Figure 3.7 is –

$$\Delta\sigma_v = \frac{q}{\pi}\left[\left(\frac{a+b}{a}\right)(\alpha_1+\alpha_2)-\frac{b}{a}\alpha_2\right] \tag{3.1}$$

The increase in vertical stress was calculated for each stage construction height of the trial embankment. In determining the incremental stress ($\Delta\sigma v$) the unit weight of the trial embankment was taken as 20kN/m3. For the condition of one-dimensional consolidation, the total effective ($\Delta\sigma_v + \sigma_v'$) stress in the soft clay layer is the summation of the insitu vertical stress and incremental vertical stress for each depth. A plot of the incremental and total effective stress is shown in Figures 3.4 (a) and (b), Figures 3.5 (a) and (b), and Figures 3.6 (a) and (b) for each construction stage.

Table 3.2: Stage 1 construction (Embankment height = 2m)

Depth (m)	$\Delta\sigma_v+\sigma_v'$ (kN/m^2)	m_v (m^2/MN)	c_v (m^2/year)	k_v (m/year)	BH
0.5	27.2	1.61	7.47	0.1179	BH 20
1.0	29.4	1.61	6.66	0.1051	
1.5	31.6	1.62	5.86	0.0930	BH 20A
2.0	33.8	1.62	5.06	0.0803	
2.5	35.9	1.72	0.54	0.0091	BH 20C
3.0	38.0	1.83	0.45	0.0080	
3.5	40.1	1.86	0.35	0.0064	
4.0	42.1	1.83	0.26	0.0046	
4.5	44.2	1.40	0.58	0.0080	BH 21E
5.0	46.2	1.43	0.56	0.0078	
5.5	48.4	1.45	0.54	0.0076	
6.0	50.4	1.51	0.52	0.0076	
6.5	52.6	1.48	0.50	0.0072	
7.0	54.7	1.50	0.47	0.0070	
7.5	57.0	1.51	0.45	0.0067	
8.0	59.2	1.52	0.43	0.0064	
8.5	61.6	0.78	0.96	0.0073	BH 21J
9.0	63.9	0.81	0.90	0.0071	
9.5	66.5	0.82	0.83	0.0067	
10.0	68.9	0.89	0.77	0.0067	
10.5	71.6	0.90	0.70	0.0062	
11.0	74.3	0.91	0.63	0.0056	
11.5	77.1	0.65	2.22	0.0141	BH 23M
12.0	79.9	0.68	2.37	0.0157	
12.5	82.7	0.70	2.51	0.0173	
13.0	85.7	0.72	2.67	0.0189	
13.5	88.7	0.74	2.83	0.0205	
14.0	91.7	0.72	2.99	0.0210	

Table 3.3: Stage 2 construction (Embankment height = 2.5m)

Depth (m)	$\Delta\sigma_v+\sigma_v'$ (kN/m^2)	m_v (m^2/MN)	c_v (m^2/year)	k_v (m/year)	BH
0.5	32.2	1.59	5.64	0.0879	BH 20
1.0	34.4	1.70	4.84	0.0805	
1.5	36.6	1.70	4.04	0.0670	BH 20A
2.0	38.7	1.79	3.27	0.0574	
2.5	40.8	1.83	0.32	0.0057	BH 20C
3.0	42.7	1.87	0.27	0.0050	
3.5	44.7	1.96	0.27	0.0052	
4.0	46.6	2.04	0.27	0.0055	
4.5	48.6	1.44	0.54	0.0076	BH 21E
5.0	50.4	1.51	0.52	0.0076	
5.5	52.5	1.49	0.50	0.0072	
6.0	54.3	1.51	0.48	0.0071	
6.5	56.4	1.52	0.46	0.0068	
7.0	58.4	1.51	0.44	0.0064	
7.5	60.6	1.49	0.41	0.0060	
8.0	62.6	1.47	0.39	0.0057	
8.5	64.9	0.79	0.88	0.0068	BH 21J
9.0	67.1	0.86	0.82	0.0069	
9.5	69.5	0.88	0.75	0.0065	
10.0	71.8	0.90	0.69	0.0061	
10.5	74.5	0.91	0.62	0.0055	
11.0	77.0	0.96	0.56	0.0052	
11.5	79.8	0.68	2.36	0.0157	BH 23M
12.0	82.4	0.70	2.50	0.0172	
12.5	85.2	0.73	2.65	0.0188	
13.0	88.1	0.75	2.80	0.0205	
13.5	91.1	0.72	2.96	0.0209	
14.0	94.0	0.74	3.11	0.0226	

Table 3.4: Stage 2 construction (Embankment height = 4m)

Depth (m)	$\Delta\sigma_v+\sigma_v'$ (kN/m$_2$)	m_v (m^2/MN)	c_v (m^2/year)	k_v (m/year)	BH
0.5	47.2	2.01	2.05	0.0404	BH 20
1.0	49.2	2.00	1.98	0.0388	
1.5	51.1	2.00	1.91	0.0375	BH 20A
2.0	52.6	2.01	1.86	0.0367	
2.5	54.1	2.04	0.28	0.0056	BH 20C
3.0	55.4	2.04	0.28	0.0056	
3.5	56.7	2.09	0.28	0.0057	
4.0	57.9	2.09	0.28	0.0058	
4.5	59.3	1.52	0.43	0.0064	BH 21E
5.0	60.5	1.49	0.41	0.0060	
5.5	62.0	1.48	0.40	0.0058	
6.0	63.4	1.51	0.39	0.0057	
6.5	65.0	1.54	0.37	0.0056	
7.0	66.5	1.53	0.35	0.0053	
7.5	68.3	1.55	0.34	0.0051	
8.0	70.0	1.57	0.32	0.0049	
8.5	71.9	0.89	0.69	0.0060	BH 21J
9.0	73.8	0.91	0.64	0.0058	
9.5	75.9	0.93	0.59	0.0054	
10.0	77.9	0.99	0.53	0.0052	
10.5	80.3	1.00	0.47	0.0046	
11.0	82.6	1.01	0.41	0.0041	
11.5	85.2	0.73	2.65	0.0190	BH 23M
12.0	87.7	0.75	2.78	0.0204	
12.5	90.3	0.73	2.92	0.0208	
13.0	93.0	0.75	3.06	0.0224	
13.5	95.8	0.73	3.21	0.0228	
14.0	98.5	0.74	3.35	0.0245	

Once the total effective stress beneath the embankment is known, the coefficient of volume decrease (m_v) can be determined. Using Figure 3.3 and the following expression –

$$m_v = \frac{1}{1+e_0}\left(\frac{e_0 - e_1}{\sigma_1^{'} - \sigma_0^{'}}\right) \tag{3.2}$$

The coefficient of volume decrease (m_v) was calculated for various depth intervals beneath the trial embankment.

The coefficient of consolidation (c_v) was also determined for various depth intervals beneath the embankment. These values were determined by linear interpolating between the QDMR laboratory c_v values (Appendix A) and the total effective stress values beneath the embankment.

With the coefficient of volume decrease (m_v) and coefficient of consolidation (c_v) known, the coefficient of permeability (k_v) for each depth interval can be calculated from the proceeding formula -

$$k_v = c_v \bullet m_v \bullet \gamma_w \tag{3.3}$$

The variation of m_v, c_v and k_v with depth is shown in Figures 3.4 (c), (d) and (e), Figures 3.5 (c), (d) and (e), and Figures 3.6 (c), (d) and (e) for each construction stage, respectively. The raw data used to produce these plots is displayed in Table 3.2, 3.3 and 3.4. The coloured figures in these tables are obtained from the stated bore holes. The uncoloured figures are the assumed distribution.

It can be seen, when referring to Figures 3.4, 3.5 and 3.6, that the coefficient of volume decrease (m_v), coefficient of consolidation (c_v) and coefficient of permeability (k_v) varies with depth. A single value for each of these parameters is required for the total soft clay strata. To determine the equivalent coefficient of volume decrease (M_v), coefficient of permeability (K_v) and coefficient of consolidation (C_v) for the whole clay layer the following procedure was followed –

i. Integrate the area under the incremental stress depth curves using the trapezoidal rule (Table 3.5), as displayed below

$$Area = \Delta\sigma_v H = \frac{\Delta H}{2}\left(\Delta\sigma_0 + 2\Delta\sigma_1 + 2\Delta\sigma_2 + \cdots + 2\Delta\sigma_{n-1} + \Delta\sigma_n\right) \tag{3.4}$$

ii. Determine the total settlement of the clay layer (Table 3.6) by summing the vertical settlement in the depth intervals, using the following expression –

$$\rho_c = \sum_{i=1}^{n} m_{vi}\Delta H_i \Delta\sigma_{vi} \tag{3.5}$$

Table 3.5: Area beneath incremental stress curves

	Height (m)		
	2	2.5	4
Depth (m)	Δσv (kN/m^2)	Δσv (kN/m^2)	Δσv (kN/m^2)
0.5	20.00	25.00	39.97
1.0	19.98	24.97	39.78
1.5	19.94	24.90	39.36
2.0	19.86	24.77	38.72
2.5	19.74	24.58	37.91
3.0	19.58	24.32	36.98
3.5	19.37	24.00	35.98
4.0	19.12	23.63	34.94
4.5	18.83	23.20	33.88
5.0	18.51	22.74	32.82
5.5	18.16	22.25	31.77
6.0	17.80	21.74	30.75
6.5	17.42	21.22	29.75
7.0	17.03	20.69	28.79
7.5	16.63	20.16	27.86
8.0	16.23	19.63	26.96
8.5	15.84	19.11	26.10
9.0	15.44	18.60	25.28
9.5	15.06	18.11	24.50
10.0	14.68	17.62	23.74
10.5	14.31	17.15	23.03
11.0	13.95	16.70	22.34
11.5	13.60	16.26	21.69
12.0	13.26	15.83	21.06
12.5	12.93	15.42	20.47
13.0	12.61	15.03	19.90
13.5	12.31	14.65	19.36
14.0	12.01	14.28	18.84
Area (kN/m)	224.1	273.5	391.6

Table 3.6: Layer settlement for different embankment heights

	Height (m)			
	2	2.5	4	
Depth (m)	ρ(mm)	ρ(mm)	ρ(mm)	BH
0.5	16	20	40	BH 20
1.0	16	21	40	
1.5	16	21	39	BH 20A
2.0	16	22	39	
2.5	17	22	39	BH 20C
3.0	18	23	38	
3.5	18	23	38	
4.0	18	24	36	
4.5	13	17	26	BH 21E
5.0	13	17	24	
5.5	13	17	24	
6.0	13	16	23	
6.5	13	16	23	
7.0	13	16	22	
7.5	13	15	22	
8.0	12	14	21	
8.5	6	8	12	BH 21J
9.0	6	8	12	
9.5	6	8	11	
10.0	7	8	12	
10.5	6	8	12	
11.0	6	8	11	
11.5	4	6	8	BH 23M
12.0	4	6	8	
12.5	5	6	7	
13.0	5	6	7	
13.5	5	5	7	
14.0	4	5	7	

Note: In the above table the coloured figures are obtained from the stated bore holes. The uncoloured figures are the assumed distribution.

iii. Once these two parameters are known, the equivalent coefficient of volume decrease (M_v) can be determined from the proceeding expression –

$$M_v = \frac{\rho_c}{Area} \tag{3.6}$$

iv. The equivalent coefficient of permeability (K_v) for the soft clay strata can be computed from the following expression -

$$K_v = \frac{\Delta H_1 + \Delta H_2 + \cdots + \Delta H_i}{\Delta H_1 / k_{v1} + \Delta H_2 / k_{v2} + \cdots + \Delta H_i / k_{vi}} \tag{3.7}$$

v. With the equivalent coefficient of volume decrease (M_v) and equivalent coefficient of permeability (K_v) known, the equivalent coefficient of consolidation can be calculated from -

$$C_v = \frac{K_v}{M_v \gamma_w} \tag{3.8}$$

The equivalent parameters for the soft clay strata, for stage 1 and stage 2 construction are displayed in the below figure –

Table 3.7: Equivalent soft clay layer parameters

	Height (m)	Mv (m2/MN)	Cv (m2/year)	Kv (m/year)
Stage 1	2.0	1.35	0.70	0.0093
Stage 2	2.5	1.41	0.62	0.0085
Stage 2	4.0	1.55	0.50	0.0076

3.5.1 Predicted one dimensional settlement

Once the coefficient of consolidation (C_v) is known, conventional design methods can be utilised to predict the settlement of the soft clay layer. Before the settlement can be calculated, the degree of consolidation (U_{av}) must first be determined. R.E. Olson's (1977) mathematical solution was used to determine the degree of consolidation of the soft clay layer –

For $T_v \le T_c$:

$$U_{av} = \frac{T_v}{T_c}\left\{1 - \frac{2}{T_v}\sum_{m=0}^{m=\infty}\frac{1}{M^4}\left[1 - \exp\left(-M^2 T_v\right)\right]\right\} \tag{3.9}$$

For $T_v > T_c$:

$$U_{av} = 1 - \frac{2}{T_c}\sum_{m=0}^{m=\infty}\frac{1}{M^4}\left[\exp\left(M^2 T_c\right)\right]\exp\left(-M^2 T_v\right) \tag{3.10}$$

When referring to Figure 3.8 the variation of the vertical time factor (T_v) against the average degree of consolidation (U_{av}) for various construction time factor (T_c) values is illustrated. From the knowledge of the Principal Geotechnical Testing Officer at QDMR, it took approximately 35 days to construct each stage of the trial embankment. For a construction time of 35 days, the corresponding T_c value is 0.001 (Figure 3.8). Using this curve and the total soft clay layer settlement (ρ_c), the settlement at any time (ρ_t) can be calculated from the following expression –

$$\rho_t = U_{av}\rho_c \tag{3.11}$$

The predicted settlement time plots for stage 1 and stage 2 construction of the embankment are illustrated in Figure 3.9.

3.5.2 Field instrumentation

During construction of the trial embankment field instrumentation was installed to monitor its performance. The following instrumentation was installed -

i. Settlement gauges
ii. Horizontal profile gauges
iii. Inclinometers
iv. Piezometers

Settlement gauges were installed, at the centre line of the embankment, to monitor vertical settlement. The surface and subsurface vertical settlement time plots for the trial embankment with no ground improvement, stone columns at 2m spacing and stone columns at 3m spacing is shown in Figure 3.10.1 (Taylor) and Figure 3.10.2 (Casagrande).

Across the base of the embankment, horizontal profile gauges were installed to record the horizontal settlement profile of the embankment. When referring to Figure 3.11, 3.12 and 3.13 the variation of vertical settlement, at regular intervals, across the embankment is shown. Also obtained from these readings, is the horizontal settlement time profile for all three embankments - Figure 3.14, 3.15 and 3.16. Polynomial aggression curves (solid lines) were fitted to the data series of these figures. The dotted curves which extend from the aggression curves are the predicted horizontal settlement profile.

Inclinometers were installed at the toe of the embankment to monitor lateral displacement. The variation of lateral displacement with depth, for the embankment with no ground improvement, stone columns at 2m spacing and stone columns at 3m spacing is shown in Figure 3.17 (a), (b) and (c) respectively.

Piezometers were installed at the centre line of the trial embankment to monitor pore pressure dissipation. The variation of pore pressure with time is shown in Figure 3.18 (a), (b) and (c) for all three embankments. It should be noted that these plots take into consideration the total excess pore pressure; which includes the static water table and the increase in pore pressure due to the construction of the embankment.

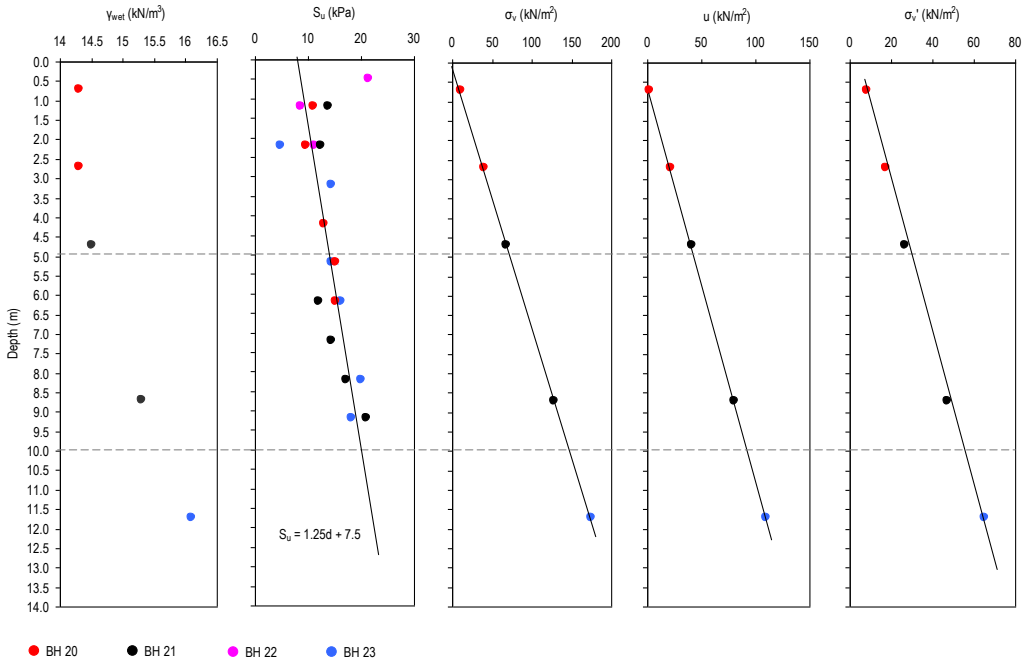

Figure 3.2: Insitu field conditions

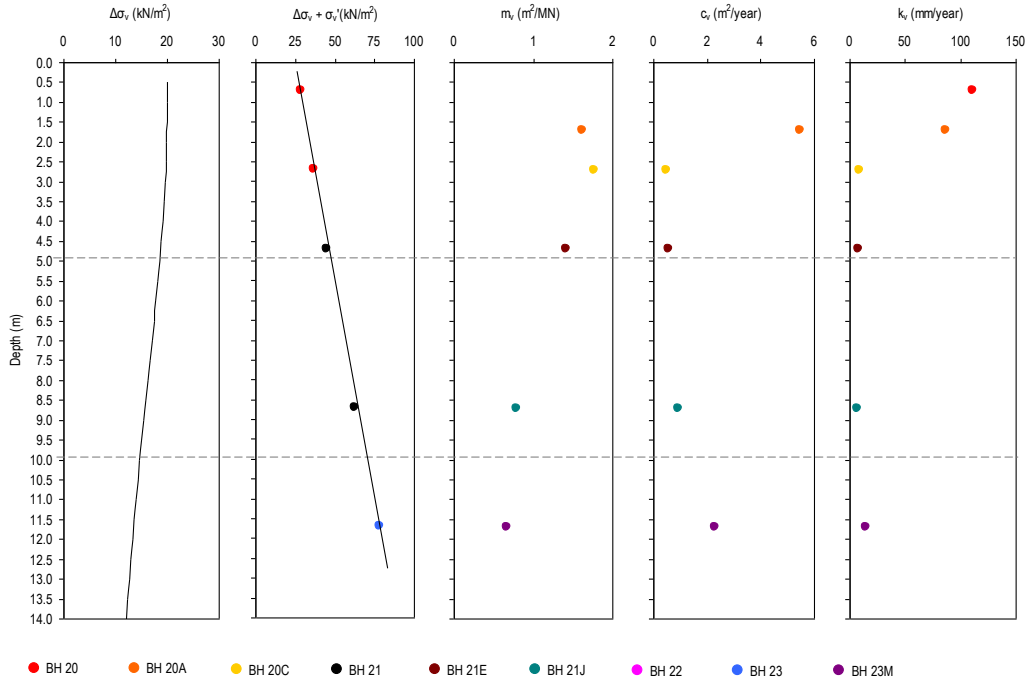

Figure 3.4: Stage 1 construction (Embankment height = 2m)

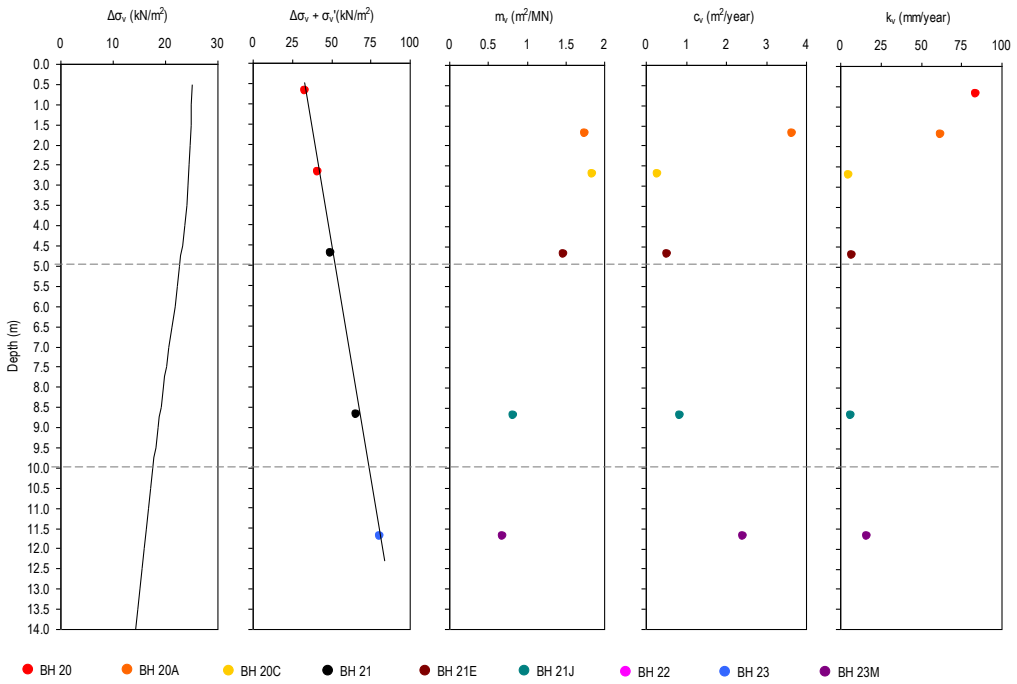

Figure 3.5: Stage 2 construction (Embankment height = 2.5m)

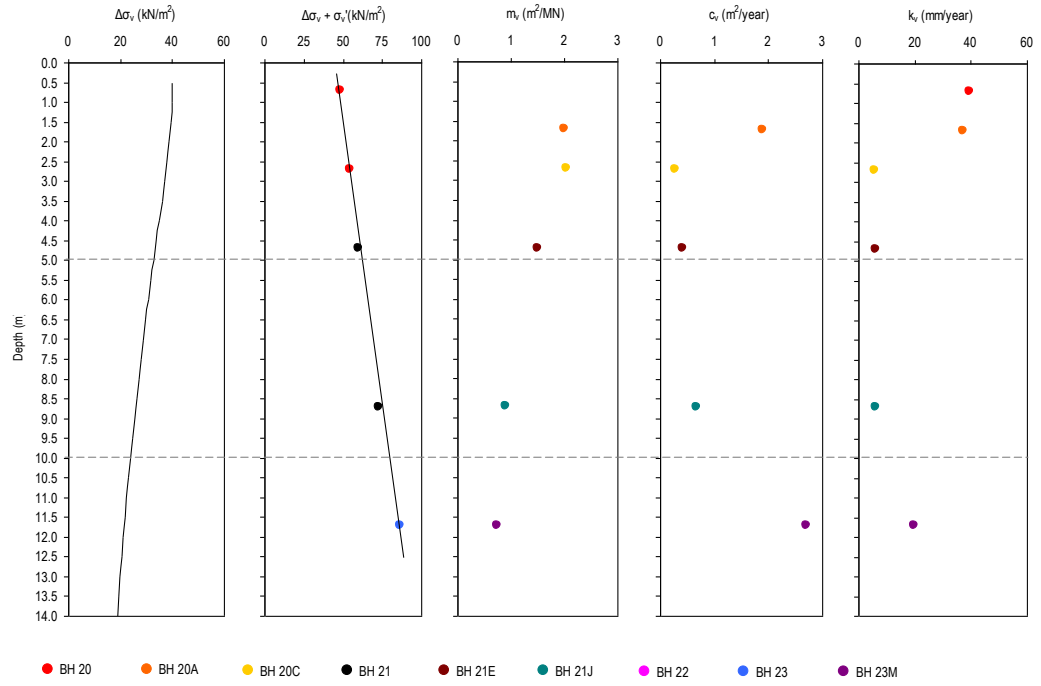

Figure 3.6: Stage 2 construction (Embankment height = 4m)

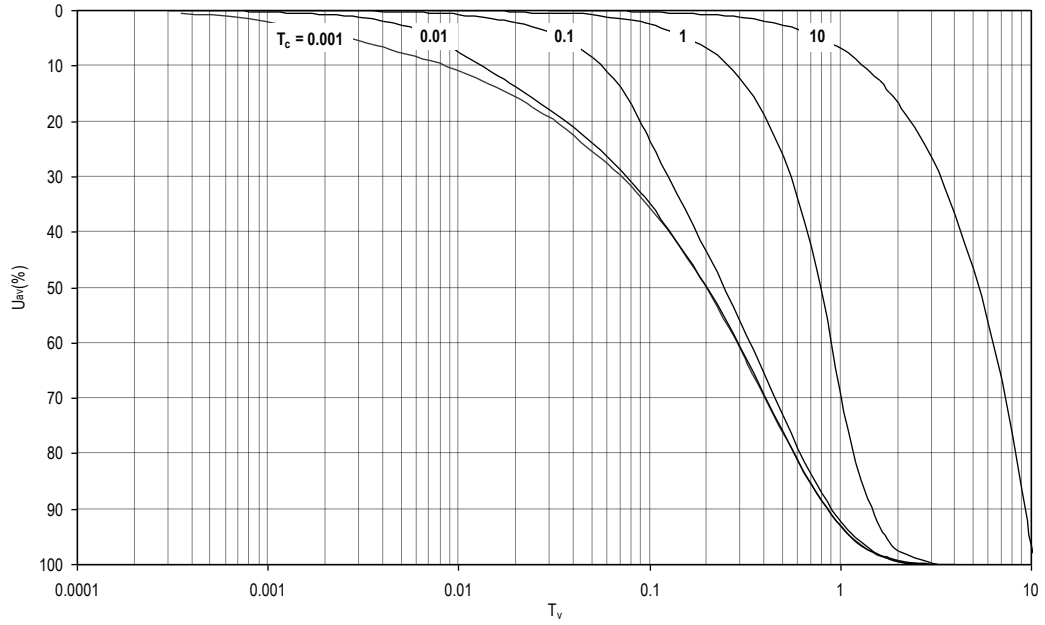

Figure 3.8: Average degree of consolidation against time factor for single ramp load

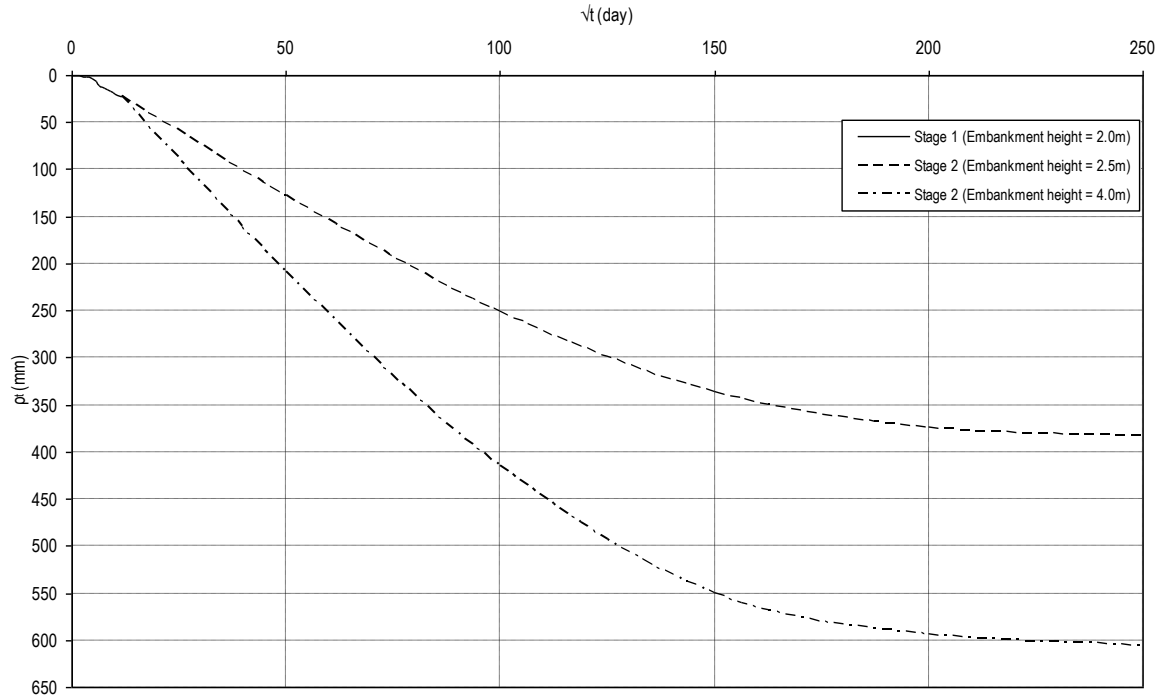

Figure 3.9: Stage 1 and Stage 2 construction one dimensional settlement time plots

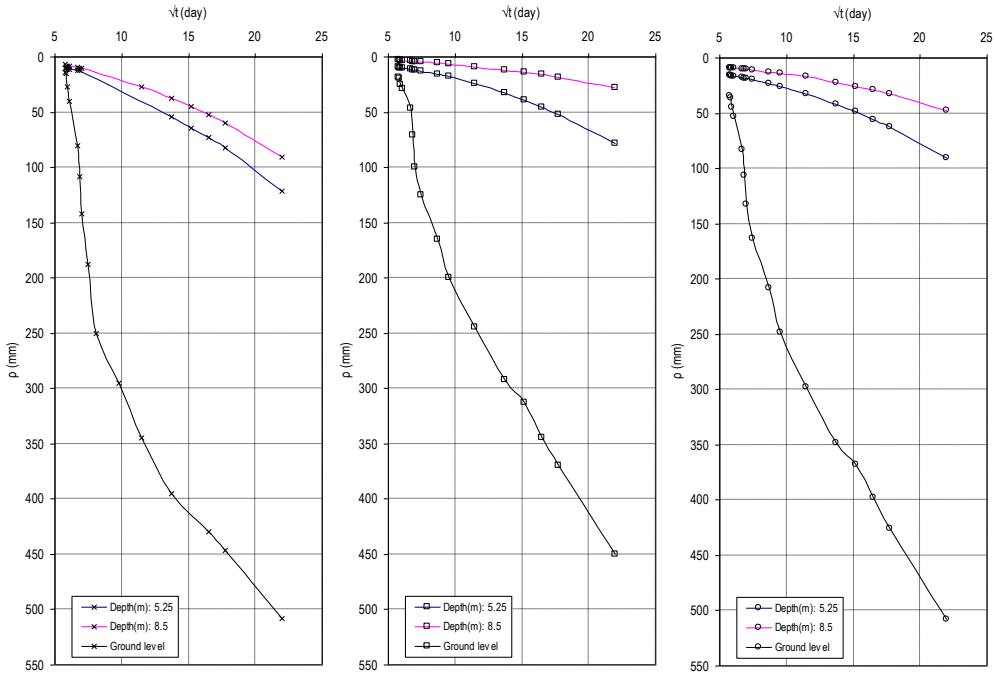

Figure 3.10.1: Settlement time plots at the trial embankment centre line (Taylor)

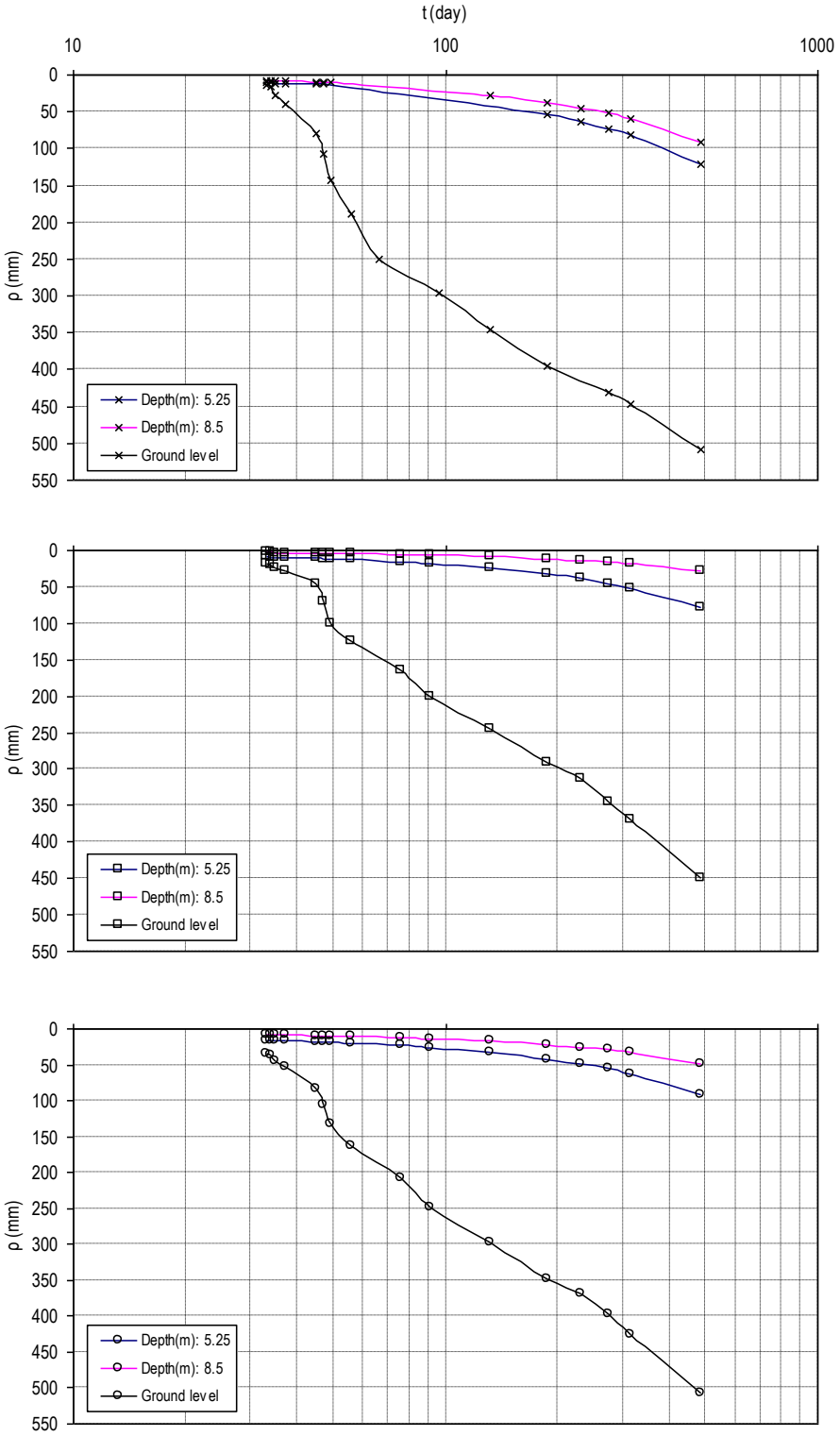

Figure 3.10.2: Settlement time plots at the trial embankment centre line (Casagrande)

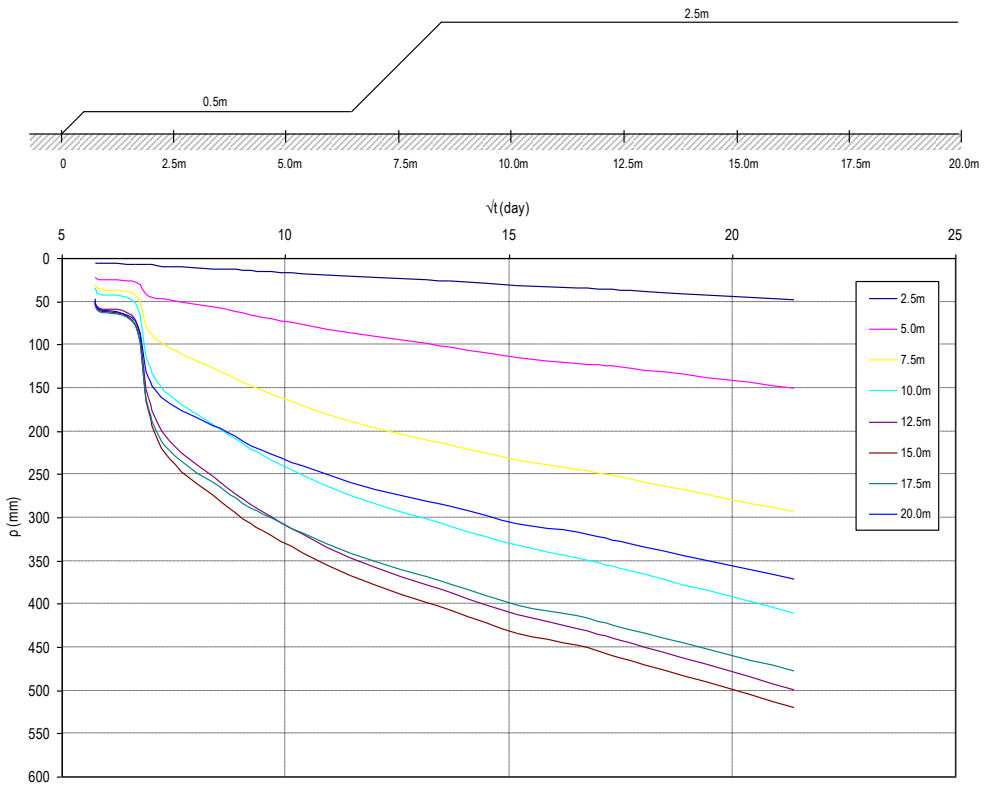

Figure 3.11: Insitu vertical settlement profile at various distances along the embankment with no ground improvement

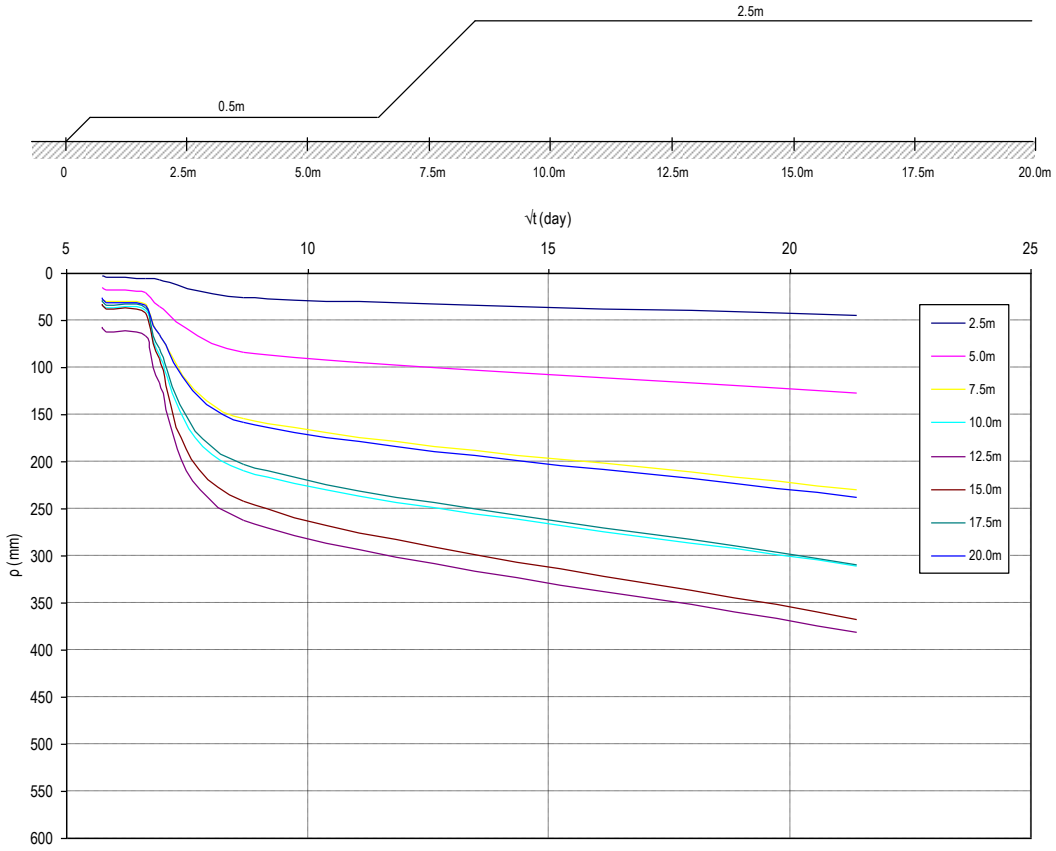

Figure 3.12: Insitu vertical settlement profile at various distances along the embankment with stone columns at 2m spacing

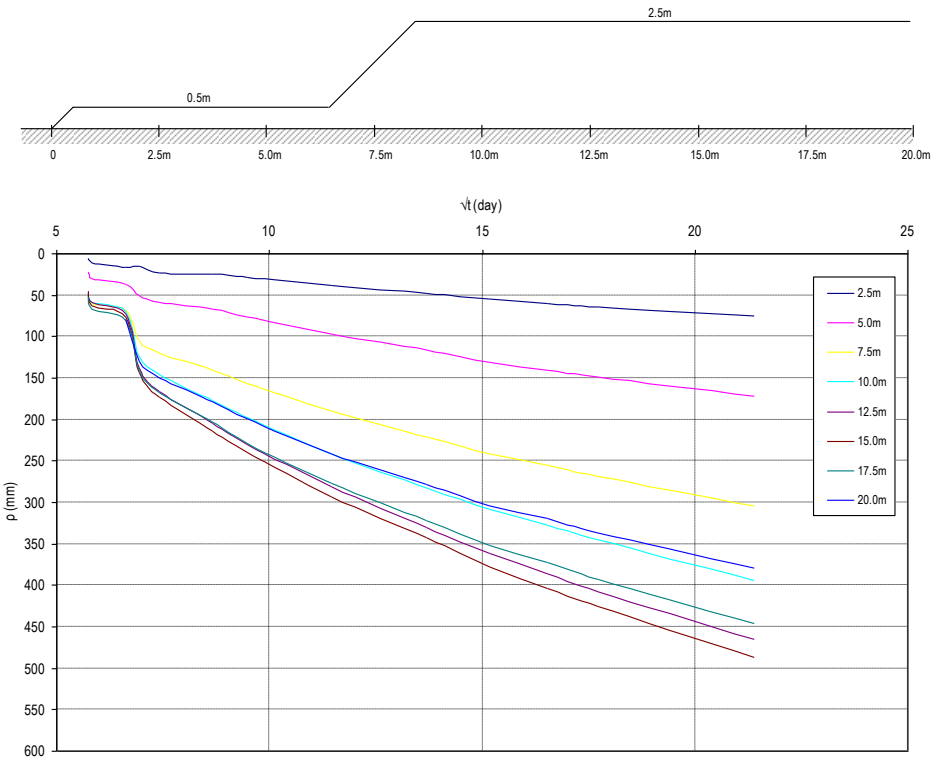

Figure 3.13: Insitu vertical settlement profile at various distances along the embankment with stone columns at 3m spacing

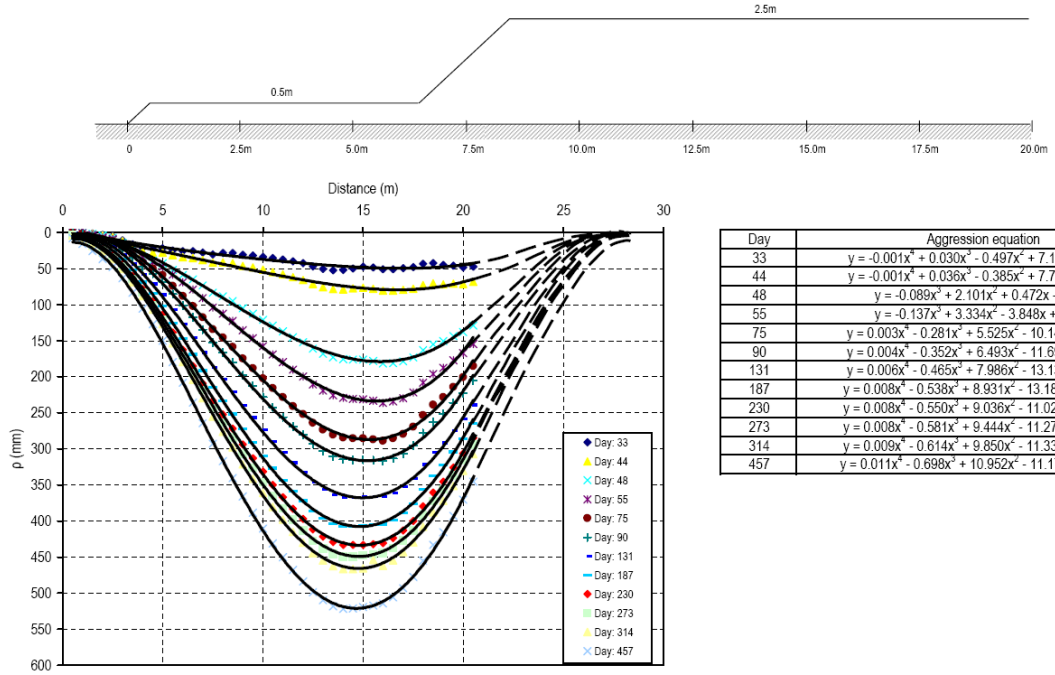

Day	Aggression equation
33	$y = -0.001x^4 + 0.030x^3 - 0.497x^2 + 7.122x - 5.822$
44	$y = -0.001x^4 + 0.036x^3 - 0.385x^2 + 7.704x - 6.114$
48	$y = -0.089x^3 + 2.101x^2 + 0.472x - 1.743$
55	$y = -0.137x^3 + 3.334x^2 - 3.848x + 1.860$
75	$y = 0.003x^4 - 0.281x^3 + 5.525x^2 - 10.141x + 7.697$
90	$y = 0.004x^4 - 0.352x^3 + 6.493x^2 - 11.691x + 8.783$
131	$y = 0.006x^4 - 0.465x^3 + 7.986x^2 - 13.134x + 9.735$
187	$y = 0.008x^4 - 0.538x^3 + 8.931x^2 - 13.185x + 10.233$
230	$y = 0.008x^4 - 0.550x^3 + 9.036x^2 - 11.024x + 10.371$
273	$y = 0.008x^4 - 0.581x^3 + 9.444x^2 - 11.278x + 11.710$
314	$y = 0.009x^4 - 0.614x^3 + 9.850x^2 - 11.330x + 12.312$
457	$y = 0.011x^4 - 0.698x^3 + 10.952x^2 - 11.177x + 16.635$

Figure 3.14: Insitu horizontal settlement time profile for the embankment with no ground improvement

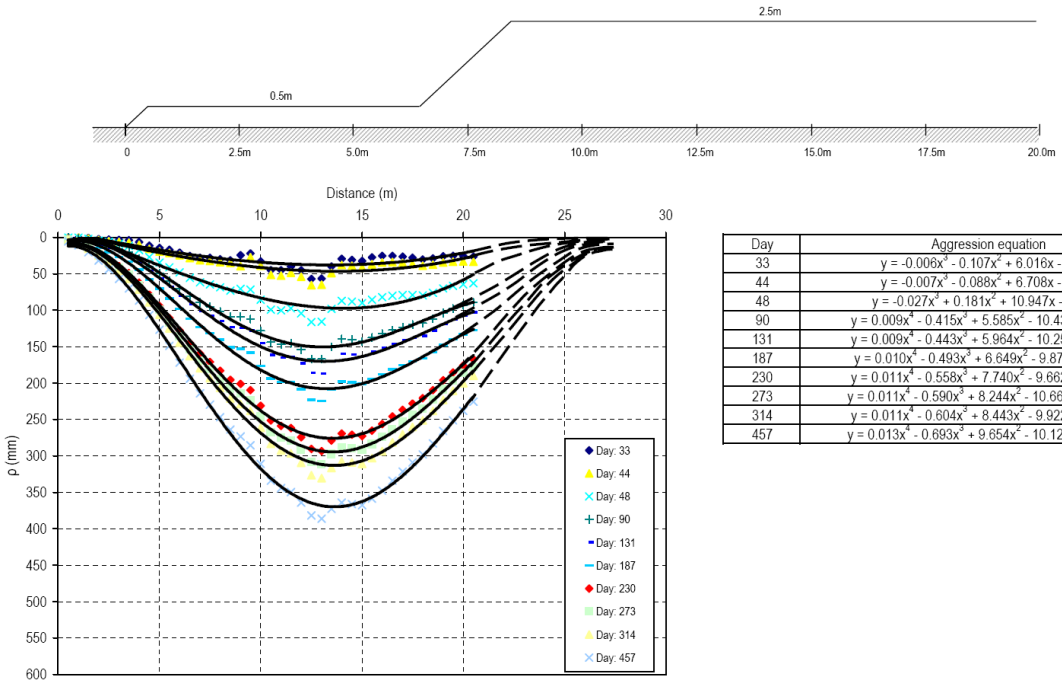

Day	Aggression equation
33	$y = -0.006x^3 - 0.107x^2 + 6.016x - 9.336$
44	$y = -0.007x^3 - 0.088x^2 + 6.708x - 9.201$
48	$y = -0.027x^3 + 0.181x^2 + 10.947x - 17.361$
90	$y = 0.009x^4 - 0.415x^3 + 5.585x^2 - 10.430x + 7.500$
131	$y = 0.009x^4 - 0.443x^3 + 5.964x^2 - 10.255x + 7.673$
187	$y = 0.010x^4 - 0.493x^3 + 6.649x^2 - 9.874x + 8.470$
230	$y = 0.011x^4 - 0.558x^3 + 7.740x^2 - 9.662x + 10.850$
273	$y = 0.011x^4 - 0.590x^3 + 8.244x^2 - 10.668x + 12.133$
314	$y = 0.011x^4 - 0.604x^3 + 8.443x^2 - 9.922x + 12.328$
457	$y = 0.013x^4 - 0.693x^3 + 9.654x^2 - 10.123x + 14.700$

Figure 3.15: Insitu horizontal settlement time profile for the embankment with stone columns at 2m spacing

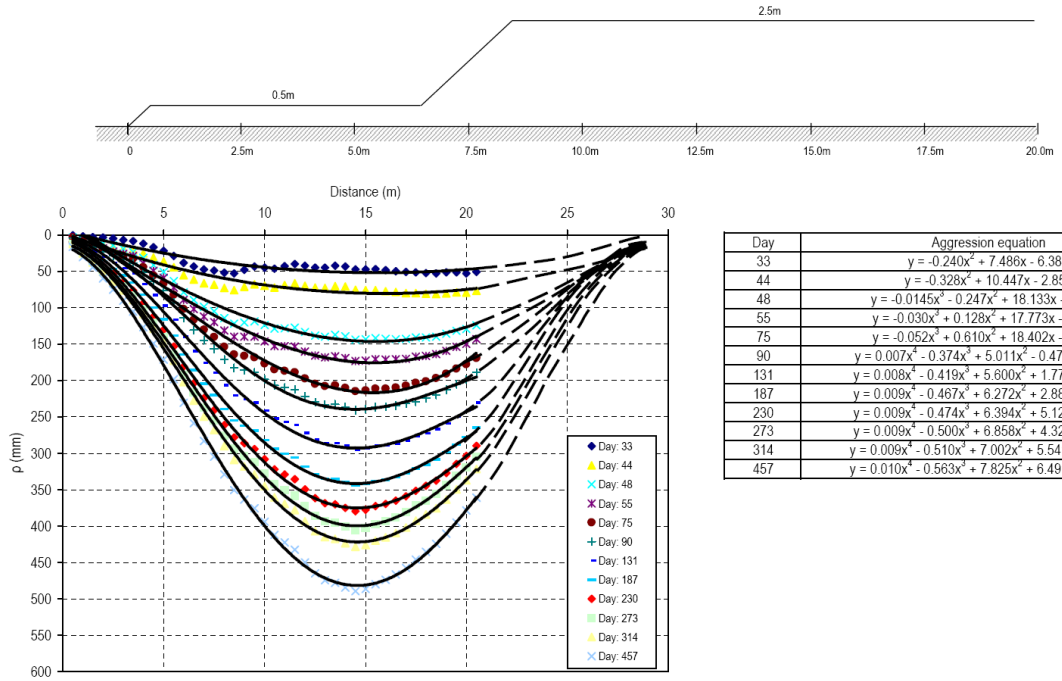

Day	Aggression equation
33	$y = -0.240x^2 + 7.486x - 6.383$
44	$y = -0.328x^2 + 10.447x - 2.850$
48	$y = -0.0145x^3 - 0.247x^2 + 18.133x - 21.112$
55	$y = -0.030x^3 + 0.128x^2 + 17.773x - 17.245$
75	$y = -0.052x^3 + 0.610x^2 + 18.402x - 19.953$
90	$y = 0.007x^4 - 0.374x^3 + 5.011x^2 - 0.474x + 3.583$
131	$y = 0.008x^4 - 0.419x^3 + 5.600x^2 + 1.777x + 4.151$
187	$y = 0.009x^4 - 0.467x^3 + 6.272x^2 + 2.884x + 6.191$
230	$y = 0.009x^4 - 0.474x^3 + 6.394x^2 + 5.123x + 6.684$
273	$y = 0.009x^4 - 0.500x^3 + 6.858x^2 + 4.323x + 11.69$
314	$y = 0.009x^4 - 0.510x^3 + 7.002x^2 + 5.541x + 11.347$
457	$y = 0.010x^4 - 0.563x^3 + 7.825x^2 + 6.491x + 15.158$

Figure 3.16: Insitu horizontal settlement time profile for the embankment with stone columns at 3m spacing

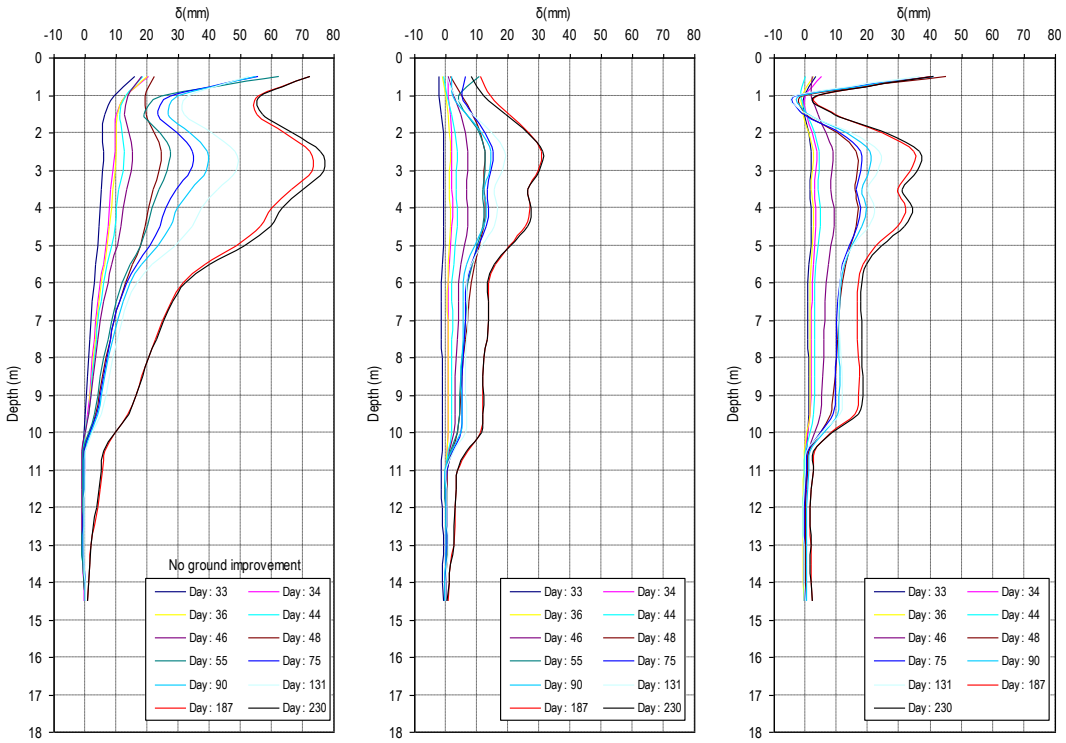

Figure 3.17: Insitu lateral displacement at the toe of the embankment

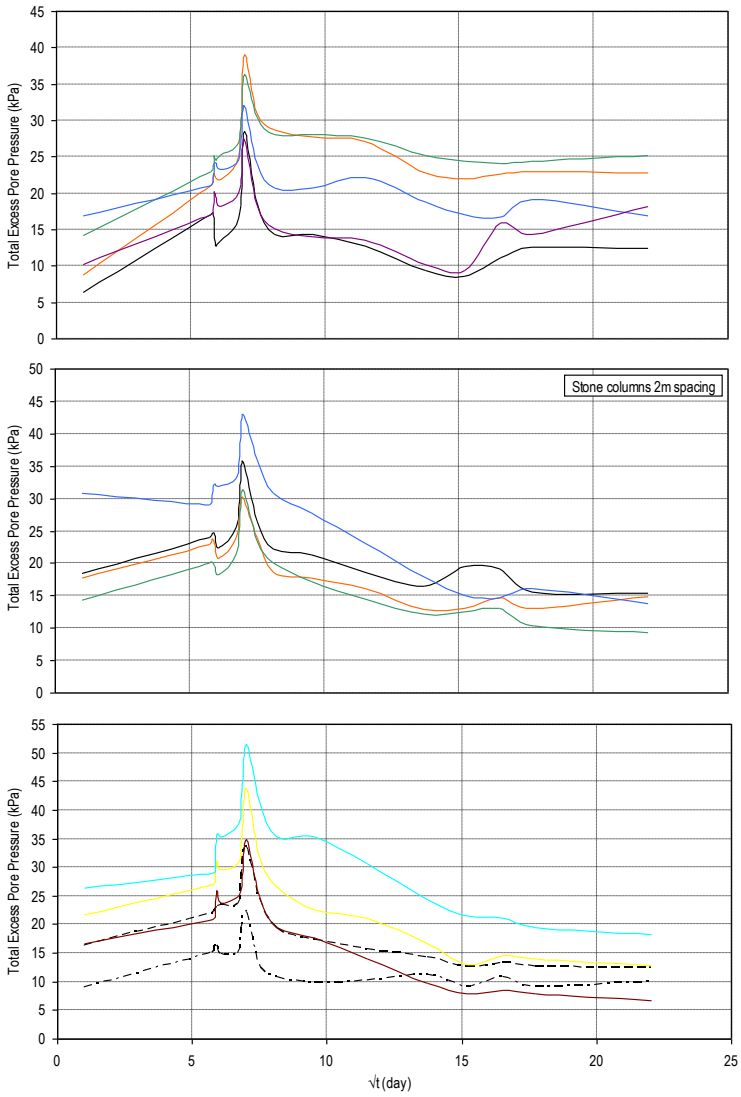

Figure 3.18: Total excess pore pressure time plots

CHAPTER 4: ANALYSIS AND DISCUSSION

4.0 Introduction

In Chapter 4 a detailed analysis of all laboratory and instrumentation data is provided. Insight is given into the measured behaviour of the trial embankment. Comparisons are made between the monitored field performances of the embankment, against the expected behaviour as envisaged during the design stage. The performance of the trial embankment was also assessed using commercial Geotechnical Engineering software packages (Slope/W & Plaxis).

4.1 Vertical settlement

4.1.1 Vertical settlement at embankment centre line

From the laboratory results, the settlement of the trial embankment was predicted for each construction stage. The predicted one dimensional settlement time plots are shown in Figure 3.9. The solid line in Figure 3.9 is the settlement after stage 1 construction. The embankment height after stage 1 construction was 2m. Construction of stage 2 began about 100 days after the completion of stage 1. After stage 2 construction, the total embankment height was 2.5m for the embankment with no ground improvement and 4.0m for the embankments with stone columns.

When referring to Figure 3.10.1 and 3.10.2 the insitu settlement time plots at the centre line of each embankment are shown. These plots illustrate the ground level settlement of the embankment and the subsurface settlement at depths 5.25m and 8.5m. The same settlement time data was used to produce these figures, however, the plotting method is varied. Figure 3.10.1 was plotted using Taylor's square root of time method, whereas, Figure 3.10.2 was plotted using Casagrande's log time method. The ground level settlement data fits Taylor's method better than Casagrande's method. Both figures illustrate that primary consolidation has not yet been completed.

These figures illustrate that installing closely spaced stone columns reduces the amount of ground level settlement. At square root time 22 days the embankment without ground improvement and the embankment with stone columns at 3m spacing had the same ground level settlement. The subsurface settlement beneath all three embankments decreased with depth. This was expected because the upper weathered crust of the soft clay layer has low strength and is highly compressible. At square root time 22 days the embankment with no ground improvement had the greatest subsurface settlement (Figure 3.10.1(a)). At the same time interval, the embankment with stone columns at 2m spacing had reduced settlement compared to the embankment with stone columns at 3m spacing. This further illustrates that closely spaced stone columns reduce the amount of subsurface settlement.

The predicted settlement of the trial embankment (Figure 3.9) is under estimated when compared to the measured settlement (Figure 3.10.1 and 3.10.2). The main reason the settlement was under estimated was due to the large variation in the magnitude of the laboratory and in-situ coefficient of consolidation.

For all three construction heights, the equivalent laboratory coefficient of consolidation (C_v) varied between 0.5 – 0.7m^2/year (Table 3.1). The in-situ coefficient of consolidation was determined, for the Coombabah Creek site by Coffey Geosciences Pty Ltd, to be approximately twenty times greater than the laboratory c_v value. Such a large variation between the laboratory and in-situ coefficient of consolidation has resulted in the under estimation of the settlement. This large variation in the coefficient of consolidation highlights the importance of large scale field tests to determine the actual in-situ soil conditions.

4.1.2 Vertical settlement profile along embankment

The vertical settlement profile at various distances along the three embankments is shown in Figure 3.11, 3.12 and 3.13. This settlement profile was obtained from horizontal profile gauges installed beneath the embankment.

The actual embankment cross-section is also displayed on these figures. Initially the embankment was constructed to a berm height of 0.5m. After the berm was built, the stage 1 of construction was (height =2m) then built on top of the berm. The stage 1 construction

began at 6.5m (horizontally) and extended to 26.5m (horizontally). The centre line of the stage 1 embankment was at 16.5m (horizontally).

This construction method is illustrated in the settlement time plots. Initially the settlement was minimal with the berm constructed, however, after stage 1 construction, the amount of settlement increased at distances 7.5m and greater.

The embankment which experienced the greatest amount of vertical settlement was the embankment with no ground improvement (Figure 3.11). Similar vertical settlement was experienced in the embankment with stone columns at 3m spacing (Figure 3.13). Figure 3.12 illustrates that installing stone columns which are closely spaced reduces the amount of settlement.

4.2 Horizontal settlement profile along embankment

Also obtained from the horizontal profile gauge was the horizontal settlement profile of the three embankments shown in Figures 3.14, 3.15 and 3.16. Polynomial aggression equations have been fitted to the known data readings. The dotted curves which extend from these aggression curves, are the predicted settlement profiles.

As stated earlier, the centre line of the stage 1 embankment was at 16.5m. The peak vertical settlement occurred at approximately 15m (horizontally), for the embankments with no ground improvement and stone columns at 3m spacing. The peak vertical settlement for the embankment with stone columns at 2m spacing occurred at approximately 13m (horizontally). The maximum settlement occurred quite close to the centre line of the embankment. The settlement then decreased either side of the embankment centre line.

The settlement profile for all three embankments cannot be purely classified as consolidation settlement. This settlement is the result of the soft marine clay being unable to support the weight of the embankment. As a result, the embankment sinks in the middle, and causes soil to be heaved at the extreme ends of the embankment. This behaviour is illustrated in the below figure –

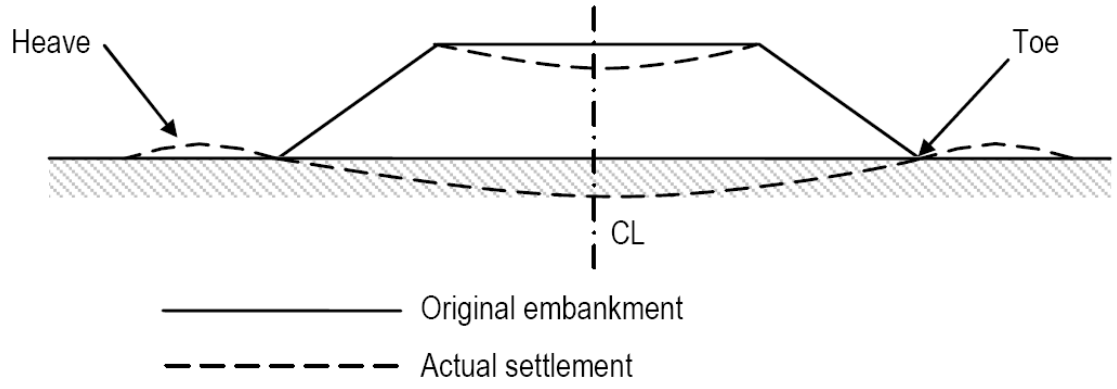

Figure 4.1: Settlement profile

This outward movement of earth from the toe of the embankment is illustrated when referring to the in-situ lateral displacement plots for the embankments.

4.3 Lateral displacement

When referring to Figure 3.17 (a), (b) and (c), the in-situ lateral displacement at the toe of the embankment with no ground improvement, stone columns at 2m spacing and stone columns at 3m spacing is shown, respectively.

These plots illustrate the variation of laterally displacement with depth, for various time increments. Nearly all of these curves move outwards from the vertical axis. This behaviour indicates instability in the trial embankment. When referring to Figure 3.17, the greatest amount of lateral displacement is experienced at depths 0 – 10m, with the lateral displacement peaking between depths 2 – 3m.

The embankment which has the greatest lateral displacement is the embankment with no ground improvement (Figure 3.17 (a)). Installing stone columns at 2m spacing reduces the amount of lateral displacement, approximately by half (Figure 3.17 (b)), when compared to the embankment with no ground improvement. The lateral displacement of the embankment with stone columns at 3m spacing (Figure 3.17 (b)), had slightly higher displacements when compared to the embankment with stone columns at 2m spacing. Thus installing stone columns beneath the trial embankment reduces lateral displacement.

4.3.1 Slope/W

The slope stability of the embankment with no ground improvement was assessed using a commercial Geotechnical Engineering software package called Slope/W. This computer program was used to determine the slip-circle failure plane and minimum factor of safety. The input parameters used in the Slope/W models are displayed in Appendix B. The Slope/W output windows are shown in Figures 4.2, 4.3 and 4.4.

The embankment stability was modelled for various embankment heights. When the embankment height was 2m (Figure 4.2), the minimum factor of safety was 1.171. The slip-circle failure plane was minimal and did not pass through the soft clay strata. Increasing the embankment height to 3m reduced the factor of safety to 1.139 and increased the size of the slip-circle failure plane. When referring to Figure 4.3 the slip-circle failure plane passed through the first 2m of the soft marine clay layer. The final modelled embankment height was 4m (Figure 4.4). The resulting minimum factor of safety was 0.904 and the slip-circle failure plane passed through the first 3m of the soft clay layer. Since the factor of safety was less than 1, the embankment was classified as unstable.

When the embankment height was 3m and 4m, the slip circle failure plane passed through depths 2m and 3m, respectively. When inclinometers were installed at the toe of the trial embankment, the peak lateral displacement was recorded between depths 2 – 3m. Thus this depth interval is the critical layer. The soil within this region has extremely low strength and low resistance to lateral movement.

4.4 Total excess pore pressure

Piezometers were installed in the trial embankment to monitor the dissipation of excess pore pressure. The variation of pore pressure with the square root of time is shown in Figure 3.18. This figure illustrates the increase and decrease in pore pressure with the construction of the

berm and stage 1 construction. It should be noted that this figure takes into consideration the static water table.

There are two peak total excess pore pressures for each embankment and each corresponding peak value occurs at a similar time (Figure 3.18 (a), (b) and (c)). The smaller peak value is from the construction of the berm and the larger peak value is from stage 1 construction.

When the berm was being constructed, the pore pressure increased with time. Once the berm was constructed the pore pressure peaked and began to dissipate with time until stage 1 construction began. When stage 1 was being built the pore pressure increased again with time until stage 1 was fully completed. The pore pressure then decreased with time until the static pore pressure was reached.

When comparing Figure 3.18 (a) with Figures 3.18 (b) and (c), the embankments with stone columns dissipate the total excess pore pressure at a faster rate than the embankment with no ground improvement. This is because stone columns behave as vertical drains and reduce the drainage length in which the pore water has to travel to be dissipated.

Piezometers are not an accurate means of measuring pore pressure dissipation. For example when considering the embankment without ground improvement at depth 8.40m, the variation of pore pressure, after peaking, fluctuates. There are two reasons which could explain this behaviour. First the height of the embankment could have been increased, resulting in an increase in pore pressure, or, there are errors with the piezometer.

4.5 In-situ coefficient of consolidation (c_v)

The following two methods were used to back calculate the coefficient of consolidation (c_v) from the large scale field test data.

4.5.1 Olson (1977) Solution

Olson's (1977) mathematical solution to determine the degree of consolidation under a time dependant load was used to determine the in-situ coefficient of consolidation of the soft clay strata. The following two expressions were used –

For $T_v \le T_c$:

$$U_e = \sum_{m=0}^{m=\infty} \frac{2q_c}{M^3 T_c} \sin\frac{Mz}{H}\left[1-\exp\left(-M^2 T_v\right)\right] \tag{4.1}$$

For $T_v > T_c$:

$$U_e = \sum_{m=0}^{m=\infty} \frac{2q_c}{M^3 T_c} \left[\exp\left(M^2 T_c\right)-1\right]\sin\frac{Mz}{H}\left[1-\exp\left(-M^2 T_v\right)\right] \tag{4.2}$$

The back calculated in-situ c_v values are displayed in Table 4.1. These values were determined from the total excess pore pressure readings after stage 1 had been fully constructed. Also the in-situ coefficient of consolidation was determined for the portion of the curve which didn't contain high increases in pore pressure.

As predicted by Coffey Geosciences Pty Ltd, the in-situ coefficient of consolidation was found to be approximately twenty times greater than the laboratory c_v value for some c_v

values. For most of c_v values determined using Olson's solution, the in-situ coefficient of consolidation was found to be much greater.

Table 4.1: Back calculated in-situ coefficient of consolidation

STAGE 1 CONSTRUCTION (EMBANKMENT HEIGHT = 2m) - NO GROUND IMPROVEMENT

	Depth (m)									
	1.40		3.40		5.40		8.40		9.90	
t(day)	u_e(kPa)	c_v (m^2/year)	u_e(kPa)	c_v (m^2/year)	u_e(kPa)	c_v (m^2/year)	u_e(kPa)	c_v (m^2/year)	u_e(kPa)	c_v (m^2/year)
49	28.60	10.44	39.02	12.48	36.44	55.12	32.08	93.37	27.40	94.43
56	18.60	25.33	31.02	38.07	30.44	84.28	24.08	134.47	18.40	153.04
66	14.30	35.30	28.73	38.11	28.15	79.10	20.78	128.77	15.10	150.82
91	14.30	22.89	27.73	27.56	28.15	51.94	20.78	84.10	14.10	105.16
132	12.70	18.73	27.12	18.69	27.54	34.68	22.18	49.57	13.49	69.93
188	9.40	22.48	22.82	18.88	25.25	27.01	18.88	40.11	10.20	58.80
231	8.62	20.70	22.04	16.17	24.46	22.65	17.10	35.41	9.42	49.60

STAGE 1 CONSTRUCTION (EMBANKMENT HEIGHT = 2m) - STONE COLUMNS SPACING = 2m

	Depth (m)							
	1.40		3.40		5.40		8.40	
t(day)	u_e(kPa)	c_v (m^2/year)	u_e(kPa)	c_v (m^2/year)	u_e(kPa)	c_v (m^2/year)	u_e(kPa)	c_v (m^2/year)
49	35.60	4.48	30.02	52.56	31.44	95.27	43.08	-
56	26.60	10.37	24.02	76.94	23.44	136.88	36.08	50.37
66	22.30	12.85	18.73	96.18	20.15	131.14	30.78	67.23
91	21.30	9.33	17.73	68.26	17.15	101.84	27.78	54.82
132	18.70	8.06	16.12	49.64	14.54	75.56	23.18	46.72
188	16.40	7.24	12.82	43.00	12.25	57.93	17.88	42.45

STAGE 1 CONSTRUCTION (EMBANKMENT HEIGHT = 2m) - STONE COLUMNS SPACING = 3m

	Depth (m)									
	1.25		3.25		5.25		8.25		9.75	
t(day)	u_e(kPa)	c_v (m^2/year)	u_e(kPa)	c_v (m^2/year)	u_e(kPa)	c_v (m^2/year)	u_e(kPa)	c_v (m^2/year)	u_e(kPa)	c_v (m^2/year)
49	22.07	16.86	33.49	32.19	43.91	-	51.55	-	34.86	45.63
56	13.07	43.80	24.49	68.07	31.91	72.27	41.55	-	24.86	99.02
66	10.77	51.10	19.20	87.24	26.62	85.78	35.25	45.84	19.57	114.43
91	9.77	40.15	17.20	67.71	22.62	72.64	35.25	30.33	17.57	85.56
132	10.16	23.73	15.59	49.46	21.01	51.17	30.64	29.31	13.96	69.35
188	11.16	13.14	14.29	36.87	16.72	44.06	24.35	29.67	9.67	62.12
231	9.09	15.70	12.51	33.95	12.93	43.91	21.57	27.82	7.88	56.58
273	10.70	9.49	13.12	27.01	14.54	33.36	21.18	23.76	8.49	45.11
314	9.09	11.28	12.51	24.46	13.93	29.78	19.57	22.41	7.88	40.66
485	9.87	6.13	12.29	15.77	12.72	20.29	18.35	15.21	6.67	28.36

4.5.2 Asaoka (1978) Solution

In 1978, Asaoka presented a new and practical approach to estimate the final consolidation settlement (ρ_∞) and in-situ coefficient of consolidation (c_v) from settlement time data for a certain time period. The following steps were completed to determine ρ_∞ and c_v –

i. Using Figure 3.10.1 the ground level settlement (ρ) at 30 day time intervals (Δt) was determined for each embankment.

ii. The settlement values ρ_1, ρ_2,…,ρ_i and ρ_2, ρ_3,…,ρ_{i+1} were then plotted as points in a coordinate system with ρ_i being the x-axis and ρ_{i+1} being the y-axis. A 45° line was also drawn.

iii. A straight line was then drawn through the data points. The location where the 45° line intersects the straight line, gives the final consolidation settlement (ρ_∞). The insitu coefficient of consolidation (c_v) is given by the following expression –

$$c_v = -\frac{5}{12} H^2 \frac{\ln \beta_1}{\Delta t} \quad (4.3)$$

The plot of the settlement values and fitted straight lines, for the three embankments, is shown in Figure 4.5 (a), (b) and (c). The in-situ coefficient of consolidation (c_v) and final consolidation settlement ($\rho\infty$) for the embankments is displayed in the below table.

Table 4.2: Asaoka's graphical method

Embankment	H (m)	Δt (day)	β_1	c_v (m^2/year)	ρ_∞ (mm)
No Ground Improvement	7	30	0.7535	70.3	520
Stone Columns 2m Spacing	7	30	0.7535	70.3	490
Stone Columns 3m Spacing	7	30	0.7535	70.3	560

The same in-situ coefficient of consolidation was obtained for all three embankments. This is many times greater than the value suggested by Coffey Geosciences Pty Ltd. Also the final consolidation settlement predicted by Asaoka's method is inaccurate. The two main functions of stone columns are to accelerate the rate of consolidation and strengthen the soft clay strata. Thus, the embankment with stone column at 3m spacing can not have a higher final consolidation settlement than the embankment without ground improvement.

4.6 Finite element embankment model

The performance of the trial embankment was also evaluated using Plaxis. Plaxis is a finite element Geotechnical Engineering computer program. This program was used to determine the consolidation settlement and lateral displacement at the toe of the embankments. Mr. P.V. Long and Mr. K. Paskkaran assisted the Author is running the Plaxis models. Mr. P.V. Long modelled stage 1 construction of the embankment with no ground improvement and the embankment with stone columns at 2m spacing. He determined the consolidation settlement at various time intervals. The input parameters used in the Plaxis model are given in Appendix C. The deformed mesh of the embankment with no ground improvement at 485 days is shown in Figure 4.6. The below tables illustrate the FEM consolidation settlements determined by Mr P.V. Long's embankment models -

Table 4.3: Embankment with no ground improvement

Elapsed time (day)	33	56	96	188	314	485
$\sqrt{t}$	5.74	7.48	9.80	13.71	17.72	22.02
FEM vertical settlement (mm)	211	248	296	356	423	484
Measured settlement (mm)	20	190	295	395	446	508

Table 4.4: Embankment with stone columns at 2m spacing

Elapsed time (day)	33	56	96	188	314	485
$\sqrt{t}$	5.74	7.48	9.80	13.71	17.72	22.02
FEM vertical settlement (mm)	291	299	312	329	352	379
Measured settlement (mm)	20	130	200	292	370	450

For day 96 and greater the finite element model (FEM) predicts the vertical settlement (Table 4.3) very close to the actual ground level settlement of the embankment with no ground improvement (Figure 3.10.1 and 3.10.2). The finite element model for the embankment with stone columns at 2m spacing (Table 4.4), over predicts the settlement for most instances, when compared to Figure 3.10.1 and 3.10.2.

Mr. K. Paskkaran modelled stage 1 construction for the embankment with no ground improvement and the embankment with stone columns at 3m spacing. These two embankment finite element meshes are shown in Figure 4.8 and 4.9 respectively. Mr. K. Paskkaran determined the lateral displacement at the toe of these embankments (Figure 4.9(a)) and the vertical movement horizontally from the embankment centre line (Figure 4.9(b)).

The lateral displacement was determined immediately after stage 1 construction and 6 months after consolidation began. When comparing the plots in Figure 4.9(a), the embankment with stone columns experiences approximately half the lateral displacement as the embankment with no ground improvement; for both time intervals. Thus stone columns reduce the amount of lateral displacement at the embankment toe.

The lateral displacement predicted by the finite element models is underestimated when compared to the in-situ lateral displacement (Figure 3.17). This is further illustrated when comparing the FEM vertical movement from the embankment centre line plots (Figure 4.9(b)) with the in-situ horizontal settlement profile (Figure 3.14 and 3.16) of the respective embankments.

Figure 4.2: Slope stability analysis (Embankment height = 2m)

Figure 4.3: Slope stability analysis (Embankment height = 3m)

Figure 4.4: Slope stability analysis (Embankment height = 4m)

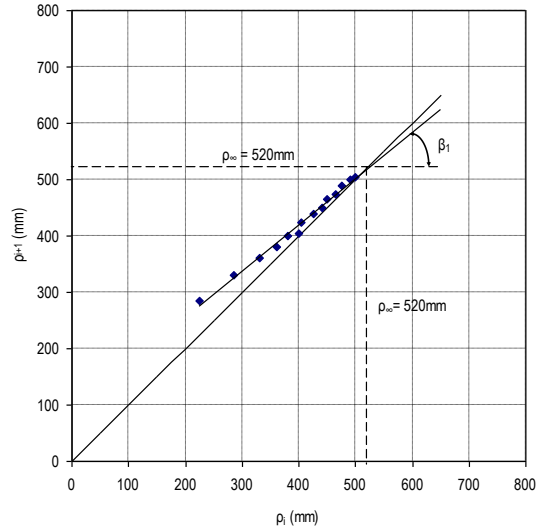

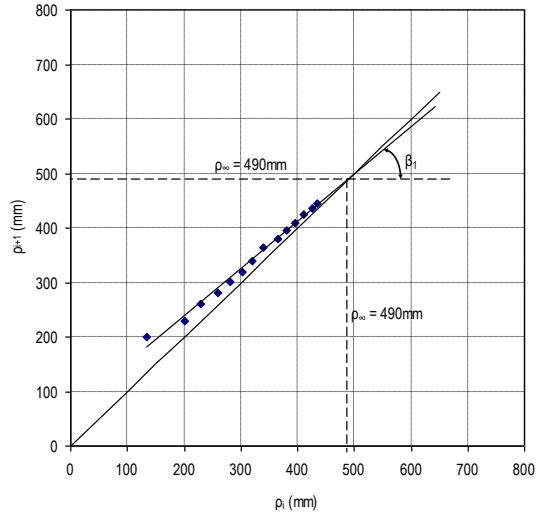

Figure 4.5a: Asaoka's method for grapical evaluation of settlement records

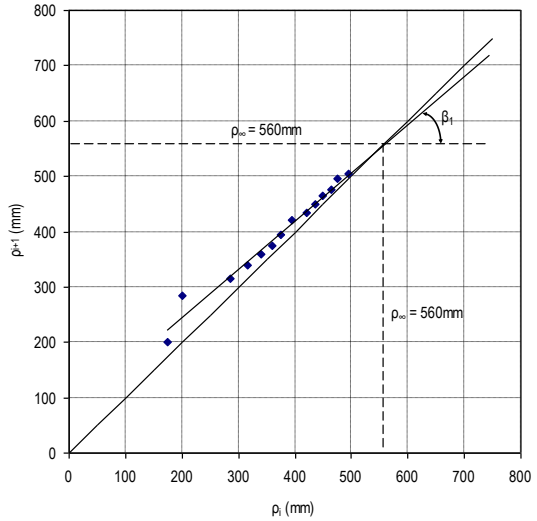

Figure 4.5b: Asaoka's method for grapical evaluation of settlement records

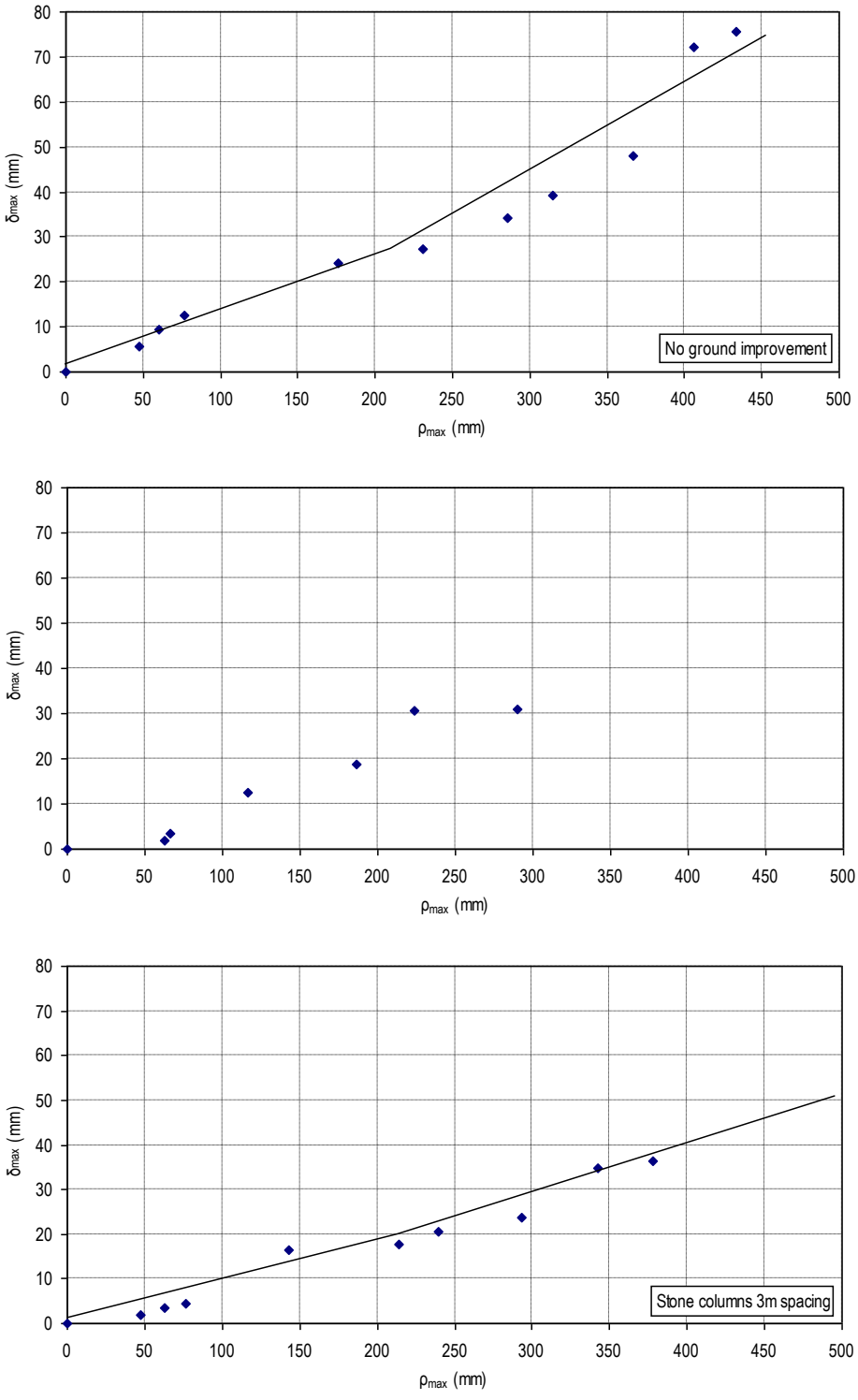

Figure 4.5: Maximum settlement against maximum lateral displacement plots

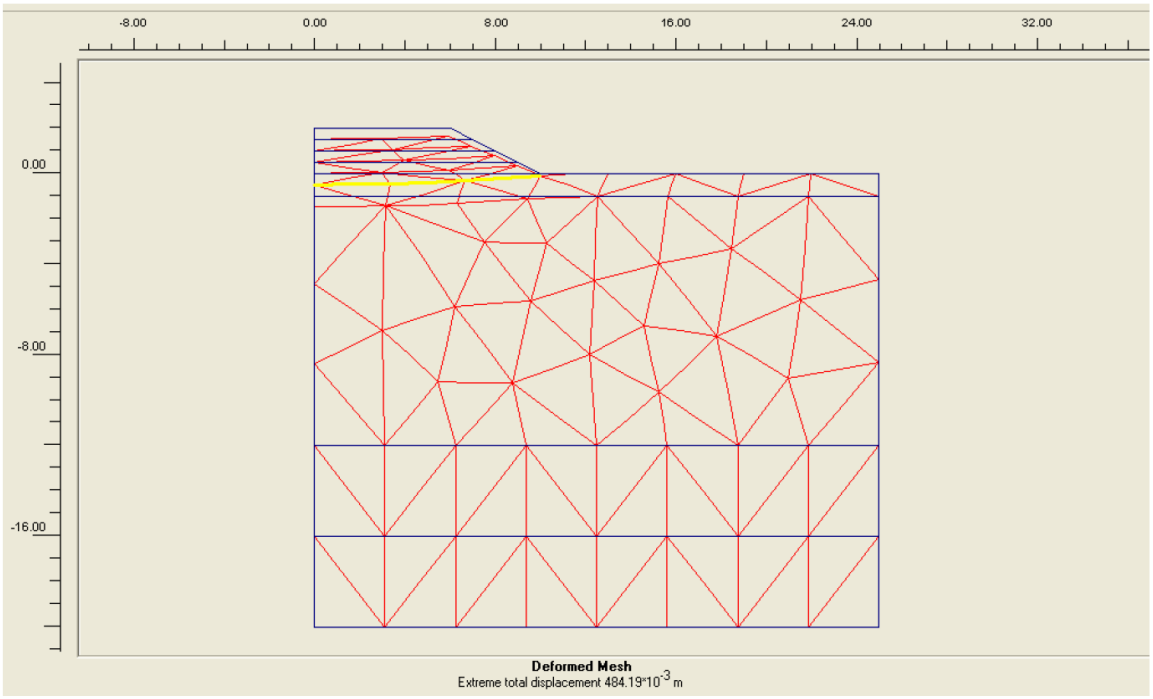

Figure 4.6: Deformed mesh of the embankment with no ground improvement at day 485 (Stage 1 Construction)

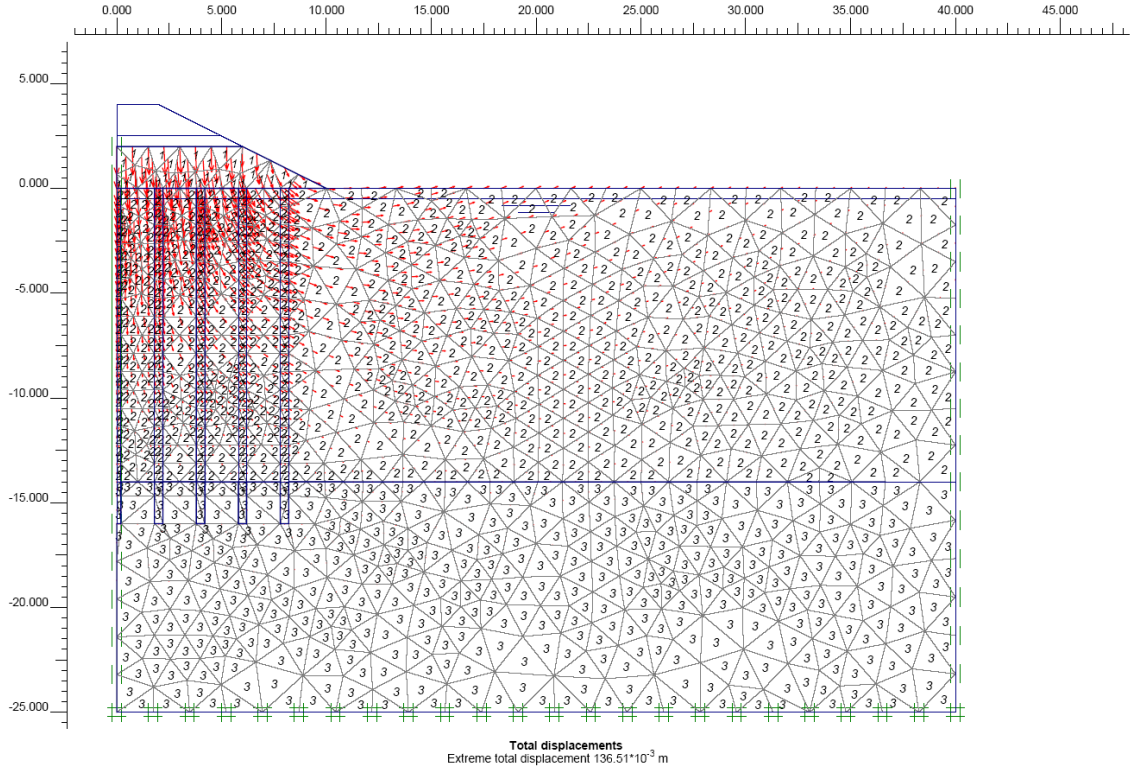

Figure 4.7: Finite element mesh for the embankment with no ground improvement (Stage 1 Construction)

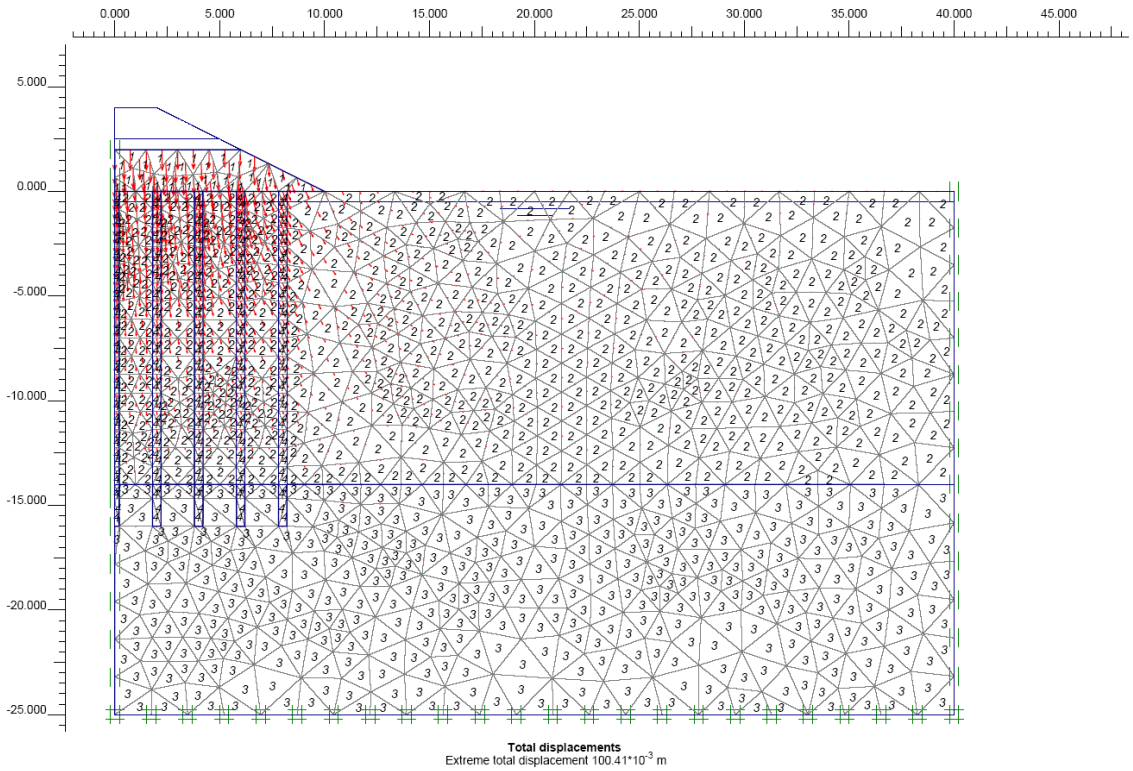

Figure 4.8: Finite element mesh for the embankment with stone columns at 3m spacing (Stage 1 Construction)

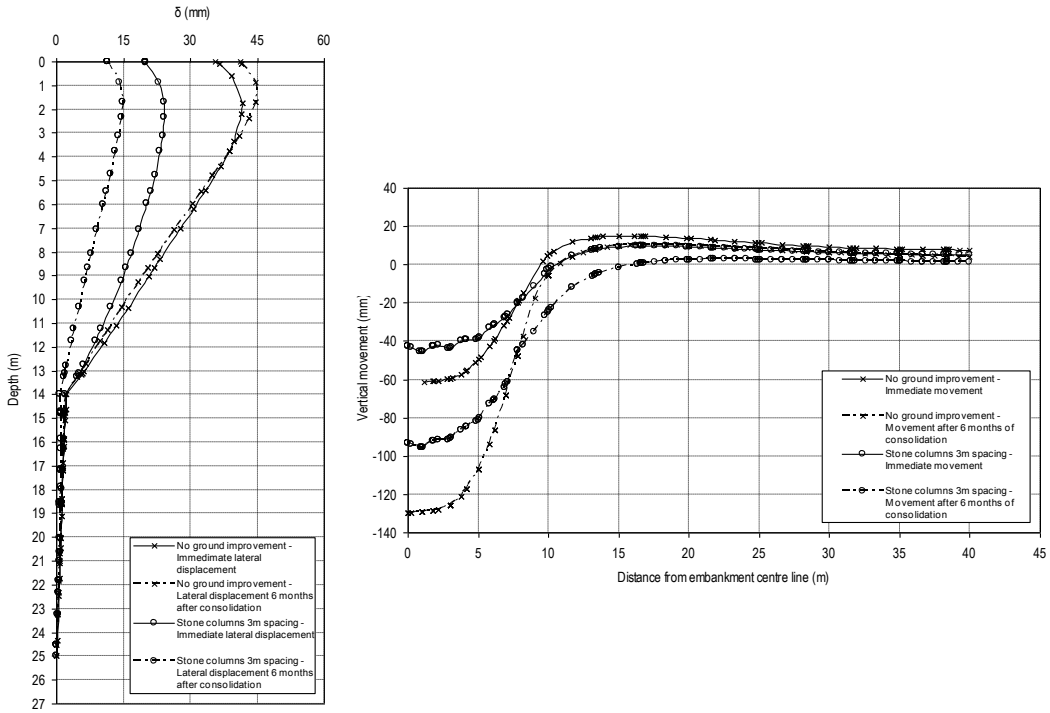

Figure 4.9: Predicted embankment movement

CHAPTER 5: CONCLUSION AND RECOMMENDATIONS

5.0 General

Construction of road embankments on soft clays poses many difficulties. The Coombabah Creek trial embankment is located in a marine environment. The water table at this site is located very close to the ground surface. The embankment was built to elevate the road from the natural flood plane and to assess the efficiency of stone columns in both reducing and accelerating the settlement of the soft organic clay.

Numerous bore holes were drilled along the proposed site and undisturbed samples taken to perform laboratory based tests. Instrumentation was installed in the trial embankment, to monitor its performance.

5.1 Summary

From the small scale laboratory tests the compressibility characteristics of the soft clay were determined. These parameters were utilised to predict the one dimensional settlement of the trial embankment. When the predicted settlement time plot was compared with the insitu settlement time plot, the predicted settlement was under estimated. Underestimation was mainly the result of the large variation between the laboratory and insitu coefficient of consolidation (cv). This variation highlights the importance of large scale field tests to determine the actual insitu soil conditions.

Settlement gauges and horizontal profile gauges were installed in the trial embankment to record the variation of vertical settlement with time. The embankment with stone columns at 2m spacing had the least settlement. The embankment with no ground improvement and stone columns at 3m spacing had comparable settlement. Since the greatest settlement of the trial embankment occurred at the embankment centre line, the insitu settlement profile can not be purely classified as consolidation settlement.

Inclinometers were installed at the toe of the embankments to monitor lateral displacement. The peak lateral displacement occurred for all three embankments between depths 2 – 3m. The slope stability of the embankment with no ground improvement was assessed using Slope/W. When the embankment height was greater than 2m, the slip-circle failure plane passed between depths 2 – 3m. This depth region was found to be the critical layer. The soil within this region has extremely low strength and low resistance to lateral movement.

Piezometers were installed in the trial embankment to monitor the dissipation of excess pore pressure. The embankments with stone columns dissipated the total excess pore pressure at a faster rate. Stone columns behave as vertical drains and reduce the length in which the pore water has to travel to be dissipated.

From the large scale field tests the insitu coefficient of consolidation (cv) was back calculated. In most instances the back calculated cv was found to be many times greater than the value suggested by Coffey Geosciences Pty Ltd.

The performance of the trial embankment was analysed using a finite element computer program called Plaxis. Plaxis was used to simulate the actual behaviour of the trial embankment. In most cases the Plaxis models either under or over estimated the actual insitu conditions.

5.2 Concluding remarks

From the extensive research into the performance of the Coombabah Creek it can be concluded that –

i. Installing stone columns at 2m centres reduces the vertical settlement
ii. Installing stone columns at 3m centres has similar vertical settlement to the embankment without ground improvement
iii. Stone columns reduce lateral displacement at the toe of the embankment by approximately half when compared to the embankment no ground improvement
iv. Stone columns accelerate the rate in which pore pressure is dissipated
v. Large scale field tests are needed to determine the actual insitu condition
vi. The reliability of FEM solutions is questionable. Engineering judgement is required to check the Plaxis model output.

5.3 Recommendations

Further research could be conducted on the Coombabah Creek trial embankment. Due to time limitations a thorough numerical analyses could not be conducted on Plaxis by the Author. For students undertaking 4091ENG Thesis, in the coming years, it is suggested that the Coombabah Creek trial embankment could be modelled on Plaxis as a thesis topic.

REFERENCES

Brand, E.W. and Brenner, R.P. (1981). Soft Clay Engineering Developments in Geotechnical Engineering, Elsevier Scientific Publishing Company, Amsterdam.

Bergado, D.T., Anderson, L.R., Miura, N. and Balasubramaniam, A.S. (1996). Soft Ground Improvement in Lowland and other Environments, ASCE Press.

Braja, D.M. (1983). Advanced Soil Mechanics, Hemisphere Publishing Corporation, USA.

Bruce, D.A. (2001). Practitioner's guide to the deep mixing method. *Ground Improvement,* **5**(3), 95-100.

Cooper, M.R. and Rose, A.N. (1999). Stone column support for an embankment on deep alluvial soils. *Proc. Instu Civ. Engrs Geotech. Engng,* **137**(1), 15-25.

Hansbo, S. (1997). Aspects of vertical drain design: Darcian or non-Darcian flow. *Géotechnique,* **47**(5), 983-992.

Indraratna, B., Bamunawita, C., Redana, I.W. and McIntosh, G. (2003). Modelling of prefabricated vertical drains in soft clay and evaluation of their effectiveness in practice. *Géotechnique,* **7**(3), 127-137.

Lee, J.S. and Pande, G.N. (1998). Analysis of stone-column reinforced foundations, *International Journal for Numerical and Analytical methods in Geomechanics,* **22**(1), 1001-1020.

Mitchell, J.K. (1981). Soil Improvement – State of the Art Report. *Proc. 10th International Conference on Soil Mechanics and Foundation Engineering Stockholm Sweden*, 509-565.

Muir Wood, D., Hu, W. and Nash, D.F.T (2000). Group effects in stone column foundations: model tests. *Géotechnique,* **50**(6), 689-698.

Wijeyakulasuriya, V., Hobbs, G. and Brandon, A. (1999). Some experience with performance monitoring of embankments on soft clays. *Proc. 8th Australia New Zealand Conference on Geomechanics Institution of Engineers Australia*, Hobart, 783 – 787.

APPENDIX A – COEFFICIENT OF CONSOLIDATION

Table A.1 Laboratory coefficient of consolidation

BH 23M						
σ_v' (kPa)	10.94	24.44	44.71	85.22	166.24	328.24
c_v (m^2/year)	5.127	4.532	0.494	2.648	0.353	0.398

BH 21J						
σ_v' (kPa)	16.87	30.31	50.48	90.80	171.45	332.73
c_v (m^2/year)	3.287	2.255	1.255	0.194	0.196	0.207

BH 20A						
σ_v' (kPa)	7.91	21.35	41.52	81.84	162.49	
c_v (m^2/year)	12.97	9.60	2.24	0.86	0.26	

BH 20C						
σ_v' (kPa)	8.05	21.55	41.82	82.33	163.35	
c_v (m^2/year)	1.09	1.20	0.27	0.30	0.28	

BH 21E						
σ_v' (kPa)	10.29	23.79	44.06	84.57	165.59	327.64
c_v (m^2/year)	4.651	4.166	0.582	0.170	0.169	0.196

APPENDIX B – SLOPE/W INPUT PARAMATERS

Table A.2 Slope/W input parameters

Description	Fill material
Soil Model	Mohr-Coulomb
Unit weight	20 kN/m³
Cohesion	0
Phi	30°
Piezometric line #	0

Description	Soft clay layer 1
Soil Model	Undrained (Phi = 0)
Unit weight	15 kN/m³
Cohesion	10 kN/m²
Piezometric line #	1

Description	Soft clay layer 2
Soil Model	S=f(depth)
Unit weight	15 kN/m³
C-Top of layer	10 kN/m²
Rate of increase	1.25
C-Maximum	25 kN/m²
Piezometric line #	1

Description	Bedrock
Soil Model	Bedrock
Piezometric line #	0

APPENDIX C – PLAXIS INPUT PARAMATERS

Table A.3 Plaxis input parameters

Description	Embankment fill
Soil model	Moh-Coulomb
φ'	30°
c'	5 kPa
γ	20 kN/m³
E'	7000 kPa
ν'	0.33

Description	Weathered crust (Uppermost 2m)
Soil model	Moh-Coulomb
φ'	23°
c'	10 kPa
γ	16 kN/m³
E'	3000 kPa
ν'	0.33
k	$2x10^{-4}$ m/day

Description	Soft clay layer (Depth 2 - 12m)
φ'	23°
c'	2 kPa
γ	14.7 kN/m³
$\lambda^* = \lambda/(1+e_0)$	0.13
$\kappa^* = 0.1\lambda^*$	0.013
OCR	1.3
k	$1x10^{-4}$ m/day

Description	Sandy sediment (12m downward)
Soil model	Moh-Coulomb
φ'	30°
c'	2 kPa
γ	18 kN/m³
E'	1000 kPa
ν'	0.25

Description	Stone columns
Model	Beam element - Elastic
E	25000 kPa